Patterns and Processes in Aerosol Bulk Deposition: Insights from a 9-year Study of ^{7}Be, ^{210}Pb, Sulfate and Major/Trace Elements

Joshua D. Landis[1], Xiahong Feng[a], James M. Kaste[2], and Carl E. Renshaw[1]

[1]Department of Earth Sciences, Dartmouth College, 6105 Fairchild Hall, Hanover, NH 03755, USA; [2]Geology Department, The College of William and Mary, McGlothlin-Street Hall 217, Williamsburg, VA 23187, USA.

Corresponding author: Joshua Landis (joshua.d.landis@dartmouth.edu)

Key Points:

1 ^{7}Be, ^{210}Pb and SO_4 in bulk deposition represent unique mixtures of distinct aerosol populations

2 primary controls on ^{7}Be:^{210}Pb ratios include airmass altitude and origin, meteorology, precipitation depth and resuspended aerosols

3 multiple aerosol populations controlling FRN deposition should be investigated for their implications to terrestrial tracer studies

Abstract

We report fallout radionuclides (FRNs) and major/trace elements (MTEs) contributions to bulk atmospheric deposition in Hanover, NH USA (43.7022° N, 72.2896° W). Deposition of ^{7}Be, ^{210}Pb and SO_4 covary [R^2>0.4, n=461] but are discriminated by production sources, depositional mechanisms, meteorological controls, MTE associations, and seasonal biases. ^{7}Be is dominated by rainout (78% of total deposition), recharged by long-range transport (+23% over mean, o.m.), influenced by stratosphere-troposphere-exchange (+9% o.m.) and solar activity (-2% per doubling of sunspot count). Correlation with particulate nitrogen (+9% per doubling of N) indicates ^{7}Be affinity for biogenic aerosols. ^{210}Pb is dominated by dry+washout deposition (54% of total) and convective storms (+107% o.m), is depleted in marine moisture sources (-133% o.m.), correlated with S (+9% per doubling of S) and biased to autumn with Mn, Hg, and V (+7% o.m.). Coincident long-term declines in S and ^{210}Pb (-14%, -4% per year) suggest co-scavenging by $PbSO_4$. ^{7}Be:^{210}Pb ratios increase asymptotically with precipitation through the dry-washout-rainout transition and recharge of ^{7}Be. These controls are expressed at the global scale through climate regimes. ^{7}Be:^{210}Pb increases with precipitation for North American/European sites due to recharge of ^{7}Be in mid-latitude storm belts [R^2=0.64, n=31]. Conversely, ^{7}Be:^{210}Pb is independent of precipitation for Southeast/East Asian sites where ^{7}Be recharge is low [R^2=0.01, n=40]. Globally, ^{7}Be:^{210}Pb ratios in dry deposition reflect resuspended aerosols with mean age of ca. 200 days, contributing <5% of ^{210}Pb deposition. Different aerosol populations contributing to FRN deposition across spatial and temporal scales should emerge as a focus in terrestrial ^{7}Be, ^{210}Pb and ^{10}Be tracer applications.

Index terms: aerosols and particles 0305, biosphere/atmosphere interactions 0426, critical zone 1402, cosmogenic nuclide exposure dating 1150, biogeochemical cycles 1615

Keywords (6): aerosol, atmosphere, beryllium-7, lead-210, fallout, sulfate

Plain Language Summary

Beryllium-7 (^{7}Be) and lead-210 (^{210}Pb) are natural radioactive elements that are produced in the atmosphere. They are powerful tools in earth and atmospheric sciences because they allow us to trace the movement of other atmospheric elements and particles such as sulfate (SO_4), toxins such as mercury (Hg), or particulate matter small enough to damage human lungs (PM2.5). After production, ^{7}Be, ^{210}Pb and associated particles reach Earth's surface in rainfall, pass through soils and sediments, and may be resuspended as dust that can pose ongoing risks of particulate exposure. To better understand how they trace atmospheric particles, we measured ^{7}Be, ^{210}Pb, SO_4 and other elements and particles in rainwater each week for 9 years. By making many measurements we were able to see important differences in how ^{7}Be, ^{210}Pb and SO_4 are delivered to the Earth's surface, and differences among other elements that they associate with. These differences are likely to have implications for how ^{7}Be and ^{210}Pb are used to date geological deposits or to measure erosion or contaminant transport, but more work will be needed to fully understand them.

1. Introduction

The natural fallout radionuclides (FRNs) ^{7}Be, ^{10}Be and ^{210}Pb are important tracers of Earth system processes. Produced in the atmosphere, they trace aerosols and atmospheric circulation (*Dibb et al. 1992, Koch et al. 1996, Delaygue et al. 2015, Liu et al. 2016, Wu et al. 2018*). Efficient removal of aerosols from the atmosphere by wet and dry deposition subsequently promotes FRNs as tracers of particle transport through terrestrial systems. There the FRNs find applications in fluvial geomorphology (*Bonniwell et al. 1999*, *Whiting et al. 2005, Evrard et al. 2010, Gartner et al. 2012, Underwood et al. 2015, Karwan et al. 2018*), lake sedimentation (*Dominik et al. 1987, Steinmann et al. 1999, Wieland et al. 1991*) and chronometry (*Krishnaswami et al. 1971*, *Appleby and Oldfield 1978*), erosion (*Wallbrink and Murray 1993, He and Walling 1996*, *Blake et al. 1999*), pedogenesis (*Kaste et al. 2011, Landis et al. 2016*), contaminant transport (*Fitzgerald et al. 2001*, *Kaste et al. 2003*, *Klaminder et al. 2006, Landis et al. 2012b, Burgos et al. 2017*) and landscape evolution (*Jungers et al. 2009, Willenbring and von Blanckenburg 2010, Wittman et al. JGR 2015*). Each of the FRNs is widely used in established applications, yet few studies combine them to exploit compelling advantages of FRN ratios. Ratios normalize changes in geochemical phase or particle size as the FRNs are redistributed through complex processes (*Barg et al. 1997*, *Wittman et al. 2015*), for example, scavenging of aerosols by precipitation (*Su and Huh 2006*), deposition from rainwater to terrestrial vegetation or soil (*Landis et al. 2012*, *2014*), or

erosion from soil to fluvial or lacustrine sediments. These ratios can also provide chronometry of aerosol and particle transport through these processes because the FRNs have different rates of radioactive decay (*Sumerling 1984, Matisoff et al. 2005, Landis et al. 2014, Landis et al. 2016*). Moreover, normalization is a critical advantage of FRN ratios because they can circumvent steady-state assumptions that are typically required by single FRN chronometers.

The challenge to exploiting FRN ratios lies in resolving ambiguities in their interpretation. FRN ratios evolve continuously with time following their production due to combinations of radioactive decay (chronometry), chemical fractionation between the FRNs (incongruence), or physical mixing between different aerosol sources (provenance). Where incongruence between FRNs can be neglected, their ratios reflect some combination of physical mixing and differential rates of decay (*Matisoff et al. 2005*). Where physical mixing between different sources can be constrained, the ratio can be interpreted unambiguously as a chronometer of atmospheric exposure (*Landis et al. 2014*, *Landis et al. 2016*). In the ideal case we would circumvent the question of congruence by choosing isotopes of the same element with identical sources, and ^{7}Be (half-life 54 days) and ^{10}Be (half-life 1.4x10^{6} years) are an obvious pair. Unfortunately, lengthy sample preparation and high costs of ^{10}Be analysis by accelerator mass spectrometry (AMS) are prohibitive for generating large data sets. The ^{10}Be half-life spanning geologic time can also complicate interpretation of ^{7}Be:^{10}Be ratios when incorporating sources with old ^{10}Be (inheritance). As an alternative, ^{210}Pb (half-life =22.3) years shares an atmospheric source with ^{7,10}Be, has a half-life consistent with contemporary processes, and is measured cost-effectively and concurrently with ^{7}Be by gamma spectrometry. [We note that due to their shared production source and identical chemical behaviors (e.g., *Wieland et al. 1991*, *Kaste and Baskaran 2011*), ^{7}Be can be interpreted as a proxy for ^{10}Be and we invoke this assumption with the abbreviation ^{7,10}Be].

The same arguments that promote ^{7,10}Be and ^{210}Pb each as particle tracers provide compelling support that their coupling as FRN ratios is appropriate. Both are divalent metals produced in the atmosphere by gas-to-particle conversion, ^{7,10}Be in the upper troposphere and stratosphere by cosmic spallation of ambient O and N, and ^{210}Pb in the lower troposphere by decay of ^{222}Rn (half-life 3.8 days) that naturally emanates from uranium-bearing soils and sediments. Following their production, the FRNs are rapidly scavenged by ambient aerosols (*Arnold and Al-Salih 1955*) with typical activity-weighted median aerodynamic diameters (AMAD) of approximately 0.5 um (*Winkler et al. 1998*, *Gründel and Porstendörfer 2004*). This size places them in the aerosol 'accumulation' mode with other environmentally critical aerosol constituents including SO_4 (20-30% of aerosol mass), black carbon (*Reddington et al. 2013*), anthropogenic metals, nuclear fission products, and PM2.5 (particulate matter <2.5 um diameter).

While their mutual production in the atmosphere establishes a common source for ^{7,10}Be and ^{210}Pb, we also expect the FRNs and related aerosols to share depositional pathways and entries into terrestrial systems since the processes that

remove aerosols from the atmosphere act on the basis of aerosol size (*Jaenicke 1980*). Aerosol deposition occurs by dry processes of impaction/diffusion or sedimentation in the absence of precipitation, and wet processes of washout (or below-cloud scavenging, BCS) and rainout (or within-cloud condensation nucleation) during storm events (*Seinfeld and Pandis 2016, Kim et al. 2000*, *McNeary and Baskaran 2003*). Subsequent to their deposition, chemical similarities between ^{7,10}Be and ^{210}Pb argue that their congruent behaviors and coherent sources will be maintained through transport in terrestrial systems. Each of the FRNs is characterized by empirical partition coefficients (K_D) on the order of 10^4 and is thus considered highly 'particle reactive' (*Lin et al. 2018*)-- they bind rapidly to ambient surfaces, materials and particles, and are assumed to trace bulk soils and sediments (*Robbins 1978*, *Mabit et al. 2014, Taylor et al. 2013, Ryken et al. 2018, Willenbring and von Blanckenburg 2010*). Thus, through shared processes of atmospheric production, aerosol scavenging, deposition and transport, fluxes of ^{7}Be and ^{210}Pb are strongly and universally correlated at sites around the globe (e.g., *Todd et al. 1989*, *Baskaran et al. 1993*, *Du et al. 2015*). On this basis it is argued that ^{7}Be and ^{210}Pb cannot be interpreted as independent atmospheric tracers (*Baskaran et al. 1993*, *Du et al. 2015*).

For all their broad similarities, however, ^{7,10}Be and ^{210}Pb behaviors during and after deposition have not been examined in detail (*Baskaran 2011, Taylor et al. 2013*). The ultra-low natural abundances of the FRNs, compounded by the complexity and minute physical size of aerosols, preclude traditional methods for characterizing the aerosols co-transporting them (*Sportisse 2007*, *Fuzzi et al. 2015*, *Prather et al. 2008*). Consequently, it is not known to what extent ^{7}Be, ^{10}Be and ^{210}Pb trace the same aerosol populations and processes, and the limits of our assumptions regarding congruent FRN behaviors remain untested. Some preliminary insights can be drawn from surveys of deposition that have proliferated over recent decades (reviews in *Du et al. 2015*, *Mohan et al. 2019*, *Zhang et al. 2021*). Compiled global data reveal systematic variations in ^{7}Be:^{210}Pb depositional ratios by latitude, longitude, under different meteorological conditions, airmass sources and changing seasons (*Olsen et al. 1985*, *McNeary and Baskaran 2003*, *Huh et al. 2006*, *Lee et al. 2007*, *Lozano et al. 2011*, *Duenas et al. 2017*, *Renfro et al. 2013*, *Du et al. 2015*, *Mohan et al. 2019*). To the first order, variations in ^{7}Be:^{210}Pb ratios reflect vertical and lateral mixing of different airmasses and the relative strengths of ^{7}Be and ^{210}Pb sources: ^{7}Be activity is highest at high latitudes and high altitudes (*Feeley et al. 1989, Delaygue et al. 2015*), ^{210}Pb activity is highest at continental longitudes and low altitudes (*Preiss et al. 1993, Baskaran 2011*).

More telling, however, are observations that ^{7}Be:^{210}Pb atmospheric flux ratios increase systematically with increasing precipitation (*Caillet et al. 2001*, *Gourdin et al. 2014*, *Chen et al. 2016*). This indicates that, despite their similar size distributions in PM2.5, ^{7}Be and ^{210}Pb are deposited by different mechanisms (*Caillet et al. 2001*, *Laguionie et al. 2014*). This difference has been attributed variously to different altitudes of the ^{7}Be and ^{210}Pb production sources (*Caillet et al. 2001, Huh et al. 2006*) or to different scavenging behaviors of ^{7}Be and

^{210}Pb themselves (*Chen et al. 2016*). The relevant processes in either case are poorly understood (*Sportisse 2007, Seinfeld and Pandis 2016*). Implications for post-depositional behavior of the FRNs are unknown.

Because FRN deposition and ^{7}Be:^{210}Pb ratios reflect a complex interplay of factors, fully understanding the ^{7}Be:^{210}Pb tracer requires a strategy that integrates multiple perspectives of aerosol behavior (Figure 1): (1) source effects due to different production mechanisms, divergent altitudinal profiles (*Turekian et al. 1983, Kownacka 2002, McNeary and Baskaran 2003*, *Dibb et al. 2003*) and both vertical and horizontal mixing of airmasses of different provenance (*Su et al. 2003*, *Lee et al. 2007*, *Delaygue et al. 2015*, *Brattich et al. 2015*); (2) multiple depositional mechanisms (*Flossman et al. 1985*, *Ishikawa et al. 1995*, *Caillet et al. 2001, Seinfeld and Pandis 2016*); (3) complex aerosol chemistries (*Kim et al. 2000*); (4) particle aging, resuspension, and contributions of recycled dust that are universally observed in FRN studies (*Brown et al. 1989*, *Monaghan et al. 1989*, *Marley et al. 2000, Graham et al. 2003, Graly et al. 2011, Baskaran 2011*); and (5) seasonality that characterizes each of these factors. We emphasize that through these processes FRN deposition is likely to involve mixtures of distinct aerosol populations, with unknown implications for downstream applications in aquatic and terrestrial systems. Because the ^{7}Be:^{210}Pb ratio normalizes behaviors that are shared between the FRNs, it should provide our most acute insights into differences in ^{7}Be and ^{210}Pb behaviors that are relevant to both their application as a coupled FRN ratio and their uses as individual tracers.

To evaluate the influences of multiple processes and their potential to discriminate the FRNs, here we describe a continuous, high-frequency, 9-year study of ^{7}Be and ^{210}Pb in bulk atmospheric deposition. Key aspects of this new dataset promote novel insights into FRN behaviors. First, we amass a large number of FRN observations to support robust multivariate statistical analyses, including both bulk deposition (n=462) and ambient PM10 (n=108). Next, we couple FRN observations with measurements of major and trace elements (MTE) in a directly-comparable, acid-soluble fraction, to provide additional context for interpreting the FRNs. Among MTEs we emphasize S given the predominant contribution of SO_4 to secondary aerosol mass and its role in determining aerosol pH and speciation/solubility of trace metals (*Fang et al. 2017*). Fe, Al, Mg, Ca and K are included as proxies for terrestrial dust sources, which could indicate the resuspension and recycling of FRN deposition (*Garland and Pomeroy 1992*; *Graly et al. 2011*). P may be important in aqueous speciation of Be (*Boschi and Willenbring 2016*). Mn is an important trace nutrient, forms surface-reactive Mn-oxide phases likely to influence FRN speciation, and can contribute to oxidative stress in the human lung (*Saffari et al. 2014*). Finally, we report trace metals Hg, V and Zn -- all anthropogenic pollutants with human health implications (*Ostro et al. 2007, Shafer et al. 2012*).

We proceed with three goals. First, to derive process-based interpretations of FRN deposition by leveraging a large number of observations with multivariate

statistics. Second, to provide insights into different aerosol populations that might transport and influence the post-depositional fate of FRNs ^{7,10}Be and ^{210}Pb and co-transported elements. Third, to link our understanding of these processes to published global data so that we may understand FRN deposition and ^{7}Be:^{210}Pb ratios at the synoptic scale. Our experimental approach follows a conceptual model described in Figure 1. Within this conceptual framework, we build our analysis sequentially through a series of statistical models, first using bivariate analyses to describe observed, objective patterns in FRN bulk depositional patterns. We then use a series of multiple regressions to control for increasing numbers of explanatory factors, allowing us to discriminate objective patterns in FRN behavior from those intrinsic to aerosol types or individual FRNs/MTEs, and then to infer causal processes that influence aerosol behavior (Figure SI1).

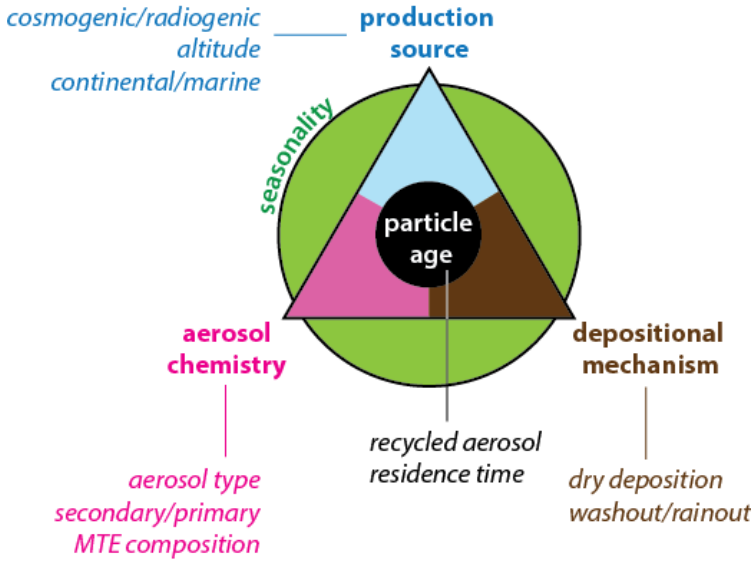

Figure 1: conceptual model of factors than may influence deposition and post-depositional behavior of aerosols including fallout radionuclides (FRNs) ^{7}Be, ^{10}Be, ^{210}Pb and major/trace elements (MTEs) including Al, Fe, C, Ca, Hg, K, Mg, Mn, N, P, S, Sr, V and Zn.

3. Methods

3.1. Study site: The study site in Hanover, NH USA (43.7022° N, 72.2896° W) sits 148 km west of the Atlantic coast at an altitude of 165 m. Local weather is strongly influenced by the polar jet and mid-latitude storm belt, with mid-latitude cyclones (MLCs) developing both at higher latitudes along continental tracks from Alaskan and Alberta Lows, and at lower latitudes with coastal tracks from Gulf and Hatteras Lows. Climate at our location is humid continental (Köppler class *DfB*), with mean annual precipitation of slightly under 100 cm and measurable precipitation recorded on an average of 2.0 days each week (no

difference in frequency by month [p=0.81] or season [p=0.74]).

3.2. Bulk deposition sample collection: We deployed tandem bulk collectors in continuous, weekly intervals in a semi-urban forest clearing at Dartmouth College, immediately adjacent to NOAA weather station USC00273850 (*NOAA*). Here we describe a continuous record spanning 9 years from March 2011 – March 2020 (n=462). Collectors were of identical polyethylene construction, trace-metal clean, with open area =650 cm^2, volume =20 L. The "A" collector was acidified following collection to recover total FRN deposition and the "B" collector was not acidified to allow speciation analyses of FRNs (described by *Landis et al. in review*). Collectors were placed at a height of 40 cm on a stable aluminum base above natural lawn to prevent toppling or rainwater splash from exposed soil. We have previously shown that this collection procedure precisely and quantitatively predicts aerosol accumulation in adjacent soils and natural vegetation (*Landis et al. 2012b, Landis et al. 2014*). Sample processing methods follow below and are illustrated in Figure SI 2.

Our "A" collector was deployed dry and acidified upon retrieval to ensure complete FRN recovery (*Baskaran 1995*). Samples were weighed for determination of precipitation amount (hereafter p_D), brought to a minimum volume of 1 liter with deionized water (if <1 liter collected), and then acidified within the collector to 2% HCl using trace-metal grade acid (Fisher Scientific). The acidified sample was turned repeatedly to rinse collector walls, then covered and rested for 7 days between collections to promote desorption of any FRNs from collector walls. The sample was then transferred to a polyethylene bottle with minimal rinsing with deionized water, reweighed, and stored at room temperature for batch processing. The procedure resulted in an effective leaching time of 4-8 weeks for insoluble particles between collection and analysis. For batch sample processing, acidified samples were filtered at 0.5 µm using tared quartz-fiber, binderless filters (47 mm diameter, Advantec QR-100) to remove insoluble particulate matter ('particulate filter'). The filtrate was processed for MTE and FRN analyses (below). Particulate filters were air-dried and weighed to measure total insoluble mass deposition (hereafter m_D). Dry collections (no precipitation) were processed identically to provide measures of bulk dry deposition.

Our "B" bulk collector was deployed in tandem to the "A" beginning in August 2017. Additional collectors were also deployed for 30 wet-only (event-based) collections. These are described in detail by *Landis et al.* (*in review*). Upon retrieval these collectors were weighed to measure p_D. Dry and trace p_D "B" collections were brought to a volume of 100 mL with deionized water, a minimum volume sufficient to rinse the collector and process the sample. For all samples a 20 mL aliquot (*a0*) was then removed for MTE analysis, filtered using a 0.45 µm nylon syringe filter and acidified with 0.5 mL concentrated HCl. The sample remainder was then filtered to tared 0.5 um quartz filters (QR-100) to remove the insoluble fraction. The filtrate was then brought to a minimum volume of 1 liter (as needed), acidified to 2% HCl and processed for FRN analysis (below). Here the "B" filtrate (<0.5 µm) represents an operationally-dissolved FRN frac-

tion, contrasting with the "A" soluble fraction. Their difference represents a 'solubility index' as the percent increase in FRN activity or MTE mass upon acidification:

$(A/B^{<0.5um}\text{-}1)$x100. Eq. 1

where A and $B^{<0.5um}$ represent the respective filtrates.

Between deployments collectors were rinsed in 2% HCl, then with deionized water (DI) 5 times, handscrubbed with Kimtech cellulose wipes (Kimberly-Clark, Irving TX), rinsed 5 times, scrubbed with Citranox detergent (Alconox, White Plains NY) using a plastic soft-bristle brush, and rinsed 30 times with DI. The collector was then filled with DI and stored for a minimum of 7 days before reuse. Prior to deployment the collectors are emptied and rinsed a further 10 times with DI to ensure no difference in pH between final collector rinse and fresh DI. Between reuse sample bottles were rinsed with DI 5 times, rinsed with Citranox solution, rinsed with DI 10 times and stored in 10% HCl for a minimum of 7 days between uses.

3.3. Ambient aerosol collection: Ambient particulate matter with aerodynamic diameters <10 µm (PM10) was collected using a PQ200 air sampler (BGI International, Waltham, MA, USA) operated continuously during 7-day collection periods at a flow rate of 16.7 L min^{-1}. Samples were collected on 47 mm quartz fiber filters (Mesa Labs, Lakewood, CO) and measured for ^{7}Be and ^{210}Pb as for bulk deposition samples.

3.4. FRN analysis: "A" and "B" samples were measured for FRN activities as follows. Each filtrate was first spiked with ^{9}Be and stable Pb tracers and an aliquot (*a1*) removed for elemental analysis. FRNs were then pre-concentrated by MnO_2 precipitation using additions of NH_4OH (*ca.* 3% by volume) to give a pH of approximately 9.5, followed sequentially by 15 µmol $MnCl_2$ and 70 µmol $KMnO_4$. After 48-hours flocculation, MnO_2 precipitates were filtered to 0.5 µm quartz fiber filters ('MnO_2 filter'). The filtration apparatus was immediately rinsed with sufficient concentrated HCl (2.5% by volume) and combined to return the filtrate to pH <1. A second aliquot (*a2*) was then removed for elemental analysis. Elemental aliquots were measured by ICPOES (Thermo Iris Intrepid II, then Spectro ARCOS beginning May 2018), and FRN yields to the MnO_2 filters were measured for each sample from ^{9}Be and Pb spike concentrations as (1-*a2*/*a1*)×100%. Yields averaged 92.3% (±3.1% 1SD) for Be and 93.1% (±3.3%) for Pb.

^{7}Be and ^{210}Pb activities on both MnO_2 and particulate filters were measured using gamma spectrometry and characteristic photoemissions at 477 keV and 46 keV, respectively. Instrumental methods follow *Landis et al.* (*2012a*). Measured FRN activities were converted to areal fluxes by normalization to the open collector area (650 cm^2) and collection duration (typically 7 days), corrected for radioactive decay to the time of collection.

We also measured ^{226}Ra and ^{228}U (via ^{234}Th) as indicators of dust contribu-

tions of 'supported' ^{210}Pb to bulk deposition. Both ^{226}Ra and ^{234}Th are co-precipitated quantitatively by the MnO_2 method. They were not detectable in individual samples, however, so we compiled a composite spectrum by summing all sample spectra (*Landis et al. 2012a*). In the composite spectrum representing >1000 days of cumulative counting ^{226}Ra was not detectable, but the maximum likely (1-sigma activity) was <1% of total measured ^{210}Pb. ^{238}U was detectable at a rate equivalent to ~1.3% of total ^{210}Pb activity. Together these low levels suggest negligible contributions of ^{210}Pb from dust sources, and that >99% of measured ^{210}Pb is atmospheric.

Gamma spectrometer calibration was performed using Canadian Certified Reference Material Project (CCRMP, Ottawa) U-ore BL5, mounted to 47 mm quartz fiber filters to provide a geometry that was identical to samples. Replicate standards were prepared using 50 mg aliquots. Identical mountings of the U,Th-ore DL1a were used for calibration verification, and agreement for all 5 detectors was within 2% of certified values. Small U-ore masses were used to prevent self-attenuation bias versus samples -- none was measurable by the point-source method (*Cutshall et al. 1983*).

We measured only a subset of the acid-leached "A" particulate filters (n=15) since none showed detectable FRN activity. Further, comparison of "A" filtrate and "B" total activities (MnO_2-plus-particulate filters) showed deficiencies in "B" samples rather than "A", averaging 10.5 ±1.5% for ^{7}Be and 13.4 ±1.9% for ^{210}Pb (mean ±SE, n=129). Deficiencies are expected due to sorption of FRNs to non-acidified collector surfaces, and by convention are omitted from speciation metrics because this fraction is not readily attributable to either particulate or dissolved fractions (e.g, *Yang et al. 2013, Huang et al. 2015*) To confirm that the 2% HCl method recovered all FRN deposition, we rinsed the "A" collector with 6N HCl in a subset of samples (n=20) following normal processing. We aggregated these rinses to improve analytical sensitivity. ^{210}Pb activity of this rinsate was equivalent to 1.3 ±0.5% of aggregate ^{210}Pb deposition, we believe most likely from residual water rather than desorption from the collector. This indicates satisfactory recovery and we thus interpret the MnO_2 filter as representing total "A" activity.

Total procedural field blanks for FRNs were routinely measured but were always below detectable limits, which are <1% of total ^{7}Be or ^{210}Pb deposition.

3.5. Major/trace elements (MTEs) analysis: Reported MTE concentrations from the "A" collector represent an acid-soluble (2% HCl) fraction, which we regard as environmentally relevant since it both replicates pH levels encountered in aerosols (~1, *Pye et al. 2019, Guo et al. 2018*) and reflects solid phases that influence aerosol chemistry and biogeochemical cycling of MTEs (*Cremean et al. 2014*, *Mahowald et al. 2017*). Acidification is moreover critical for providing insight into MTE compositions of particle surface coatings and fine aerosols that control sorption of FRNs and trace-metals (*Singleton et al. 2017*). We emphasize that measurement of MTEs in a 2% HCl fraction maintains comparability with the FRNs, since acidification is necessary for

complete recovery of FRNs from bulk deposition.

Total elemental fluxes were calculated as measured concentration times sample volume, normalized to collector area and collection duration. MTE analysis by ICPOES included the reference material NIST1640a for quality control, with recoveries expressed as a percent relative to certified value (mean ±SE, ±SD, n=27): Al (104 ±1, ±2.6%), Be (98 ±1, ±5.2%), Ca (98 ±1, ±4.0%), Cd (99 ±2, 8.1%), Co (99 ±2, 8.5%), Cr (98 ±1, ±4.6%), Cu (99 ±1, ±5.3%), Fe (101 ±5, ±6.4%), K (96 ±2, ±11%), Mg (99 ±1, ±3.8%), Mn (100 ±1, ±4.9%), Na (98 ±1, ±4.8%), Sr (99 ±1, ±3.8%), V (93 ±3, ±14%), Zn (100 ±1, ±4.4%). P or S are not certified in 1640a. S recovery for the present data set (101 ±1, ±3.9%) was consistent our own long-term mean value (1.55 µg mL^{-1}). Hg was measured by ICPMS (Agilent 7700).

Both filtration and procedural field blanks were routinely analyzed for all elements, and depositional fluxes corrected accordingly. Blank contributions were derived primarily from quartz-fiber filters because samples were filtered following acidification. On an annual basis procedural blanks contributed the following proportions to measured MTE budgets: Al (3.0%), Ba (0.6%), Ca (5.6%), Fe (2.9%), Hg (4.0%), K (1.7%), Mg (2.8%), Mn (4.1%), Na (1.3%), P (0.5%), S (1.0%), Sr (1.8%), Zn (13%). Blanks for V were not measurable but made a maximum likely (1-sigma) contribution of <12%.

Total combustible carbon (C^P) and nitrogen (N^P) were measured on "B" particulate filters using a Shimadzu combustion analyzer on 6 mm punches subsampled from particulate filters. A superscript emphasizes that these are measured on a particulate fraction, versus MTEs which are measured on soluble fractions.

3.6. Statistical analyses and multivariate methods: We combined multiple methods to describe structure in FRN/MTE data: Analysis of Variance (ANOVA), Multiple Analysis of Variance (MANOVA), Analysis of Covariance (ANCOVA) and Multiple Linear Regression. Statistical analyses were performed in JMP Pro 14.1.0. For all tests we used R^2 to report total variance in the response variable explained by the model. We report p-values to indicate statistical significance, with values <0.05 considered significant. For ANOVA we also report F-statistics to distinguish them from linear regressions. The number of observations included in each analysis is reported as n, with any omitted outliers indicated parenthetically, e.g. n=xx(y).

Multiple regression allowed us to resolve multiple, simultaneous and independent influences on FRN and MTE deposition, either multiple linear regression where only continuous variables were indicated or ANCOVA to include categorical variables. We first screened multiple regressions for significant explanators using step-wise Bayesian information criterion (BIC). Due to the high collinearity of bulk deposition parameters we took these precautions to eliminate spurious or inflated correlations among explanatory variables: first, we observed the Bonferroni correction for family-wise error so that rejecting each of m null hypotheses must satisfy $p \leq \frac{\alpha}{m}$. Next, each significant explanator was removed,

in turn, to confirm that its inclusion increased the overall model adjusted-R^2. Third, Variance Inflation Factors (VIFs) were computed for each explanator. VIF calculates the underestimation of model coefficient standard errors due to explanator multicollinearity. VIFs were computed by removing the model response variable and rotating each of i explanators, in turn, as the new response variable. VIF for each i was then calculated as: $VIF_i = 1/(1\text{-}R_i^2)$, where R_i^2 is the coefficient of determination for the VIF model. Standard errors of explanator model coefficients are inflated by a factor $=(VIF_i)^{-1/2}$, with a factor of 1.7 (corresponding to VIF >3 and R_i^2 >0.70) here considered unacceptable. In this case the explanator(s) with lesser model effect were removed. Finally, we applied step-wise k-fold validation (k=5) to ensure that R^2 of the validation set approximated R^2 of the model, an indication that the model is not overdetermined.

For accepted multiple regression models we quantified the importance of each significant explanator in two ways. We first estimated its net independent effect (e^*) on variance of the response variable as follows:

$$e_i^* = \frac{SS_i}{\sum_i^n SS} \bullet R^2 \text{ Eq. 2}$$

where SS_i is sum-of-squares for each i variable and R^2 is the total model coefficient of determination. We also estimated the magnitude of explanator effect on the response variable. For continuous variables and models of the form log(y)= $\cdot$ log(x), log-log model coefficients represent the fractional change in the response variable (called elasticity) for a given fractional change in explanatory variable. We report this magnitude (m^*) as the percent change in response variable given a 100% increase (doubling) of the explanator:

$$m^* = (2^\beta - 1) \times 100\% \text{ Eq. 3}$$

For categorical explanators we cite the difference in least-squares adjusted means (μ_i) between categories:

$$m^* = \left(10^{(\mu_1 - \mu_2)} - 1\right) \times 100\% \text{ Eq. 4}$$

3.7. Compilation of global deposition ^{7}Be, ^{210}Pb and ^{7}Be:^{210}Pb ratios

Several excellent reviews of global ^{7}Be and ^{210}Pb deposition data have appeared in recent years (*Du et al. 2015*, *Mohan et al. 2019*, *Zhang et a. 2021*). None have analyzed ^{7}Be:^{210}Pb ratios in detail, however, so we compiled sources from *Zhang et al. (2021)* for this purpose. Data sources include: *Akata et al. 2008*, *Alonso-Hernandez et al. 2014*, *Appleby et al. 2002*, *Appleby et al. 2003*, *Baskaran et al. 1993*, *Baskaran 1995*, *Baskaran and Swarzenski 2003*, *Benitez-Nelson and Buesseler 1999*, *Caillet et al. 2001*, *Chen et al. 2016*, *Cho et al. 2011*, *Clifton et al. 1995*, *Dominik et al. 1987*, *Du et al. 2015*, *Duenas et al. 2011*, *Hirose et al. 2004*, *Hu et al. 2020*, *Huh et al. 2006*, *Jia et al. 2003*, *Kim et al. 1998*, *Kim et al. 1999*, *Kim et al. 2000*, *Laguionie et al. 2014*, *Lal et al. 1979*, *Landis et al. herein*, *Lee et al. 2015*, *Leppanen 2019*, *Lozano et al. 2011*, *McNeary and Baskaran 2003*, *Mohan et al. 2019*, *Momoshima et al. 2006*, *Olsen et al. 1985*,

Peirson et al. 1966, *Peng et al. 2019*, *Pham et al. 2013*, *Renfro et al. 2013*, *Rengarajan and Sarin 2014*, *Saari et al. 2010*, *Schuler et al. 1989*, *Short et al. 2007*, *Su et al. 2003*, *Sugihara et al. 2000*, *Todd et al. 1989*, *Tokieda et al. 1996*, *Turekian et al. 1983*, *Wan et al. 2010*, *Yamamoto et al. 2006*, *Yi et al. 2005*, *Yi et al. 2007*, *Zhang et al. 2019*.

Abbreviations

$_P$ storm precipitation amount normalized by annual total

$_i$ storm FRN or MTE deposition normalized by annual total

$_i$ precipitation-normalized FRN deposition (= $_i$/ $_P$)

FRN fallout radionuclide, a particle-reactive radioactive isotope produced in the atmosphere

MTE major/trace element

p_D precipitation amount [cm]

PM2.5 particulate matter <2.5 um aerodynamic diameter

PM10 particulate matter <10 um aerodynamic diameter

m_D particulate mass deposition [mg m^{-2}]

P_C particulate concentration [mg L^{-1}]

winter December-February

spring March-May

summer June-August

autumn September-November

PC principal component, empirical orthogonal variable maximizing sample variance

v_D dry depositional velocity [m d^{-1}] (PM10 concentration normalized by measured flux)

$e*$ variance explained by an individual explanator in multiple regression

$m*$ relative magnitude of explanator effect on response variable in multiple regression

r_0 mean FRN/MTE flux by rainout mechanism [Bq m^{-2}]

w_0 mean FRN/MTE flux by washout mechanism [Bq m^{-2}]

d_0 mean FRN/MTE flux by dry deposition [Bq m^{-2}]

T_0 total FRN/MTE flux by all mechanisms [Bq m^{-2}]

N^P total particulate (combustible) nitrogen

C^P total particulate (combustible) carbon

NAE North American/European global region for FRN deposition

SEA Southeast/East Asian global region for FRN deposition

SEA-j Sea of Japan region of Southeast/East Asia

4. Results and Discussion

We begin our Results with a description of measurements in *Section 4.1.* In the following *Sections 4.2-4.6* we identify organizational structure within FRN and MTE data from the perspective of aerosol sources, chemistries, depositional processes and seasonalities (Figure 1). Next, in *Section 4.7* we integrate these different perspectives on FRN deposition using multiple regression to arrive at process-based interpretations of FRN behaviors (Figure SI2). Finally, in *Section 4.8* we place our results in a global context using compiled global deposition data.

4.1. Measured fluxes of precipitation and mass (dust), FRNs and MTEs

Over a nine-year period from 11 March 2011 through March 2020, we collected 462 weekly "A" samples of bulk atmospheric deposition for measurement of FRNs and MTEs (Table 1). Of these, 26 were free of wet deposition and were used to assess bulk dry depositional fluxes (n=26, cumulatively 182 days or 6.0% of record duration). A total of 117 "A" collections captured individual storm events and were used for meteorological analysis. Between August 2017 and August 2020, we also collected 143 non-acidified "B" samples in tandem to the "A", as well as an additional 30 event-based (wet-only) collections. Finally, we collected 126 samples of ambient aerosol <10 um (PM10) concurrently with bulk deposition collections. Multivariate plots of FRNs and MTEs in the "A" collections are shown in Figure SI 3, with breakdowns of monthly/seasonal data in Figure SI 4. We defined seasons as follows: winter = Dec.-Feb., spring = Mar.-May, summer = Jun.-Aug., autumn = Sep.-Nov.

4.1.1. Precipitation depth, mass (dust) deposition, particulate concentration and pH:

Total precipitation amount (hereafter p_D) averaged 21 mm per week but varied by both month [R^2=0.10, p<0.0001] and season [R^2=0.048, p=0.0002] with a maximum in summer (Figure SI4). Seasonal p_D totals deviated from the mean as follows (Table 2): summer $(+33\%)^{A}$ > spring $(-2\%)^{AB}$ > autumn $(-28\%)^{B}$ > winter $(-36\%)^{B}$. Connecting letters in superscript show significant differences if two seasons do not share the same letter [p<0.05]. Differences between the "A" and "B" collectors p_D totals averaged 0.01 ±0.02 cm (mean ±SD), an average difference of 0.4% and coefficient of variation (CV) = 5.1%, n=121(*15*).

Flux of insoluble aerosol or dust mass (collectively, m_D) averaged 16 g m^{-2} y^{-1}, typical of terrestrial sites with regional dust sources and higher than global

background of ~1 g m^{-2} y^{-1} measured in remote ocean basins (*Lawrence and Neff 2009*). m_D was not correlated with p_D across the full data set [linear R^2=0.003, p=0.26, n=446], but was linearly correlated for p_D greater than 1.5 cm [R^2=0.025, p=0.0029, n=227(9)]. Thus, while a dry process (dust) was the primary contributor to m_D, wet deposition of aerosols made measurable contributions as well. m_D was seasonal with a spring maximum [R^2=0.19, p<0.0001; Figure SI 4], with deviations from the mean as follows (Table 2): spring (+57%)^A > summer (-11%)^B > fall (-84%)^B > winter (-308%)^C. Difference in m_D between "A" and "B" collectors were normally distributed with an average difference of 6.3%, CV =39% (n=139(*17*)).

Median particulate mass concentration in bulk deposition (P_C) was 12 mg L^{-1}, with a flux-weighted mean of 16 mg L^{-1}. This was 4 times higher than event-based samples (4 mg L^{-1}; n=30) due to deposition of resuspended dust during dry periods that interceded precipitation events. P_C was strongly, inversely correlated with p_D [R^2=0.62, p<0.0001]. Mean annual pH of bulk deposition measured from the tandem "B" collector was 5.04 ±0.05 (geometric mean ±geometric SD, n=161, with low values in autumn (4.94 ±0.09) and winter (4.97 ±0.09), intermediate in spring (5.26 ±0.09), and highest in summer (5.39 ±0.09) (*Landis et al. in review*).

4.1.2. Deposition of FRNs: Annual ^{7}Be flux averaged 2120 ±170 Bq m^{-2}, summed from weekly measurements and corrected for decay between rainfall events and collection dates using a daily flux model (*Landis et al. 2012*). Annual flux was comparable to other mid-latitude sites with similar precipitation totals (*Du et al. 2015*). Deposition of ^{7}Be in our record was strongly predicted by p_D [R^2=0.48, p<0.0001; Figure 2]. We detected no long-term trend in ^{7}Be deposition. While measurements of ^{7}Be concentrations in ambient air have been shown to correlate with solar activity over long-term (*Aldahan et al. GRL 2008*) or short-term (*Papastefanou and Ioannidou App. Rad. Isotopes 2004*), bivariate analysis did not show a significant effect of sunspot count on ^{7}Be bulk flux [R^2=0.02, p=0.74; data source *WDC-SILSO 2019*]. Comparison of "A" and "B" collectors showed a mean difference of 15.8% due to sorption to the "B" collector, an expected and unavoidable result in speciation studies (*Yang et al. 2013*, *Huang et al. 2015*). For this comparison, CV =19% (n=135(*18*)).

Annual ^{210}Pb flux averaged 188 ±22 Bq m^{-2} y^{-1}, consistent with global databases but at the higher end of the published range (*Preiss et al. 1996, Baskaran 2011, Zhang et al. 2021*). We detected a small but significant decline in ^{210}Pb deposition over the course of the record [-3.5 ±1.4% per year, R^2=0.015, p=0.0097]. Deposition of ^{210}Pb was strongly correlated to p_D [R^2=0.32], but more strongly to deposition of ^{7}Be [R^2=0.76, Figure 2]. Equivalent ^{210}Pb steady-state inventories estimated from annual deposition (*Monaghan 1989*) were 13 ±5% higher than measured in local undisturbed soils (6200 ±190 Bq m^{-2} y^{-1}, mean ±SE, n=9 years, versus 5500 ±180 Bq m^{-2} y^{-1}, n=5 high-resolution soil pits; data from *Landis et al. 2016*). Comparison of "A" and "B" collectors showed a mean difference of 13.7%, with CV =27% (n=130(*13*)). For the ^{7}Be:^{210}Pb ratio, mean

difference was 4.6% with CV =28% (n=147(6)).

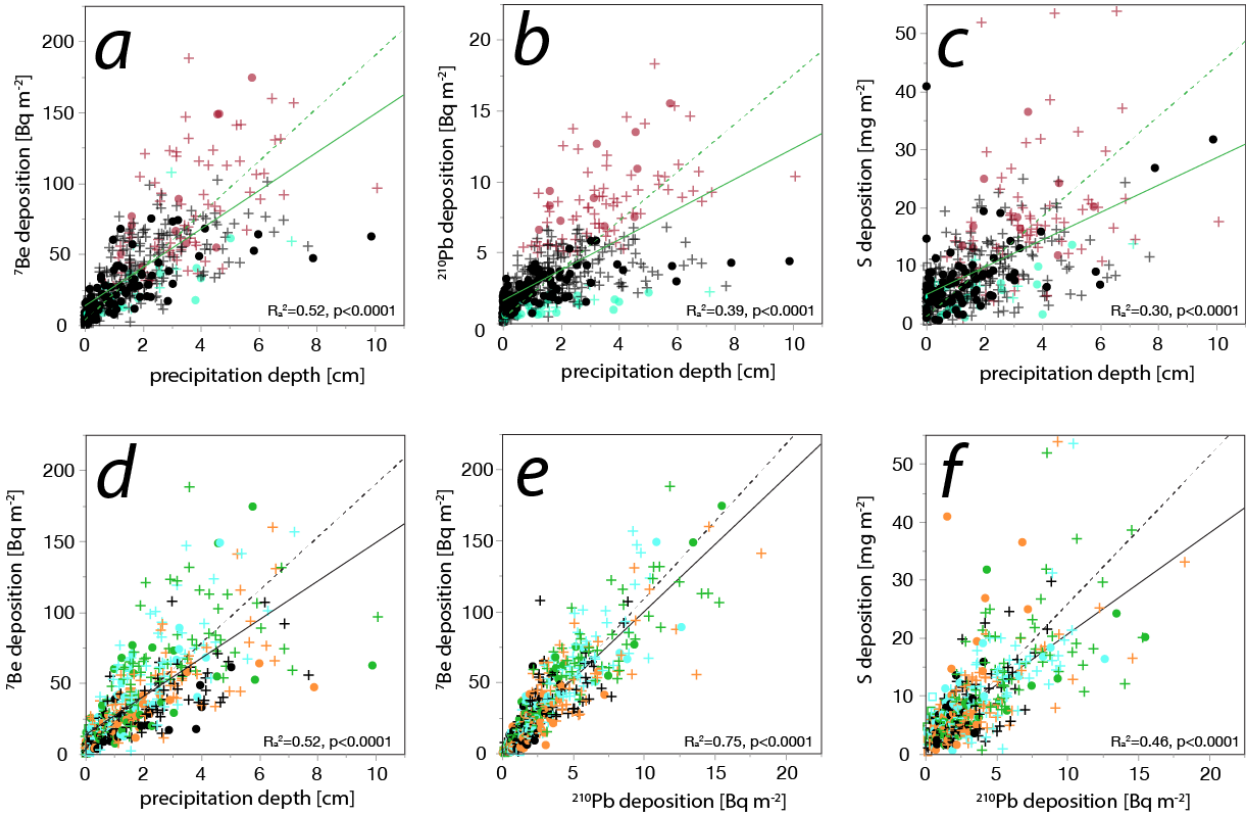

Figure 2: (a-c) fluxes of ^{7}Be, ^{210}Pb and S versus precipitation depth. Symbols are colored by storm type (*Section 4.4*), aquamarine for ^{210}Pb-depleted storms (D), red for ^{7}Be-and-^{210}Pb-enriched storms (E), or black for normal (N) storms. Circles indicate single-storm samples and crosses indicate multiple-storm samples. Single-storm N-collections are in bold. (d-f) symbols are colored by season for winter (black), spring (blue), summer (green), autumn (orange). Solid lines show linear regressions and dashed lines show orthogonal regressions.

4.1.3. Deposition of MTEs: Annual S flux declined linearly over the course of the record, from 780 mg m^{-2} in 2011-2012 to 280 mg m^{-2} in 2019-2020 [R^2=0.86, p=0.0003]. Both the magnitude and trend were comparable to wet-plus-dry deposition data for other northern New England sites (Underhill, Lye Brook, Woodstock, and Hubbard Brook; US EPA https://www.epa.gov/castnet, accessed 11/28/19). Declining S deposition reflects reduced anthropogenic emissions and is observed across North America (*Aas et al. 2019*). For subsequent analyses we detrended S data. Like ^{7}Be and ^{210}Pb, soluble S deposition was correlated with p_D [R^2=0.36, p<0.0001] but more strongly to both ^{7}Be [R^2=0.41, p<0.0001] and ^{210}Pb [R^2=0.48, p<0.0001] (Figure 2).

Because we acidify the "A" collector to ensure complete recovery of FRNs and trace metals, and collect both wet and dry deposition, soluble base cations Ca, Na, Mg and K were highly enriched in our record versus wet-only deposition at regional NADP sites (National Atmospheric Deposition Program, US EPA) by 270%, 330%, 400% and 900%, respectively. For MTEs the solubility effect is typically greater for dust constituents and lesser for secondary aerosols (e.g., NOx, SO_4; *Staelens et al. 2004*). For example, our mean dissolved-fraction P flux of 70 mg m^{-2} y^{-1} is within the range reported for North American sites (*Tipping et al. 2014*).

We quantified the solubilization of FRNs/MTEs as a percent increase in the "A" collector versus the non-acidified "B" collector = (A/B –1) x100%. For ^{7}Be and ^{210}Pb we used activities of only the <0.5 um fraction of the "B" collector to maintain comparability with the MTEs (Table 1). Solubilization increased in this order (geometric mean %):

primarily dissolved: S (*14%*) <Na (*23%*) <Zn (*48%*) <^{7}Be (*54%*) <K (*66%*) <V (*67%*) <Ca (*73%*)

intermediate: Sr (*96%*) <^{210}Pb (*104%*) <Mn (*130%*) < P (*180%*) <Mg (*210%*)

primarily solubilized: Al (*1800%*) <Fe (*2500%*)

In contrast to MTEs, acidification of the collector reduced the recovery of mass deposition by a flux-weighted average of 14 ±3% [±SE, n=132(13)] due to dissolution of particulate matter. Total soluble Al represented 0.9% of total m_D; Fe =1.9%, Ca =2.8% (geometric means). Together these suggest that the 2% HCl soluble MTE fraction is weighted to high surface-area, low-volume fine aerosols and mineral surface coatings with small contributions from large dust particles.

We found p_D to be a significant predictor of fluxes for each FRN or MTE [p<0.05, with exceptions of Al and Fe; Figure SI3]. Those with strong correlations included: ^{7}Be (R^2=0.63) >^{210}Pb (0.45) >S (0.38) >Zn (0.16) >K (0.12). Similarly, m_D was a significant predictor for deposition of each FRN/MTE [p<0.05, with exceptions of Na and Hg; Figure SI3]. Those with strong correlations were: Mg (R^2=0.45) >Fe (0.35) >Mn (0.31) >Al (0.29) >Ca (0.28) >P (0.23).

4.2. FRNs interact with five common classes of aerosol

We characterized aerosols that contributed to FRN/MTE deposition using a combination of multivariate techniques. We first used Principal Component Analysis (PCA) to separate FRN/MTE variables along empirical axes. PCA was also used to impute missing data for N^P, C^P and Hg so that these variables could be used in multiple regression without sacrificing data (*Supporting Information*). Good separation of variables was achieved using PC2 and PC3 based on summer vs. winter seasonality [R^2=0.21] and wet vs. dry deposition [R^2=0.67], respectively (Figure 3a). We followed PCA with multiple linear regression to identify the strongest independent correlations among variables and then illustrated these using Correlation Network Analysis (CNA, *Toubiana et al. 2013*) (Figure 3b).

Based on these results and details from our preceding discussion we attributed each FRN/MTE to five common classes of aerosols as shown in Figure 3 (*Belis et al. 2013*): (1) secondary aerosols include ^{7}Be, ^{210}Pb, S; (2) biogenic aerosols include C, N, Mn (*Rea et al. 2001*); P, K (*Creamean et al. 2014, Shen et al. 2019*), with correlations to S, and the combination of N, P and K also possibly indicating contributions of agricultural soils (*Tositti et al. 2018*); (3) anthropogenic aerosols include V (*Chen and Duce 1983, Shafer et al. 2012*), Hg (*Driscoll et al. 2013, Eckley et al. 2016, Jiskra et al. 2018*), Zn (*Gonzalez et al. 2016*), and Na (*Dugan et al. 2017*), with strong correlations to S (*Batonneau et al. 2004*); (4) insoluble mineral aerosols include Fe, Al; (5) soluble mineral aerosols include Mg, Ca, Sr. These are described in more detail in *Supporting Information*.

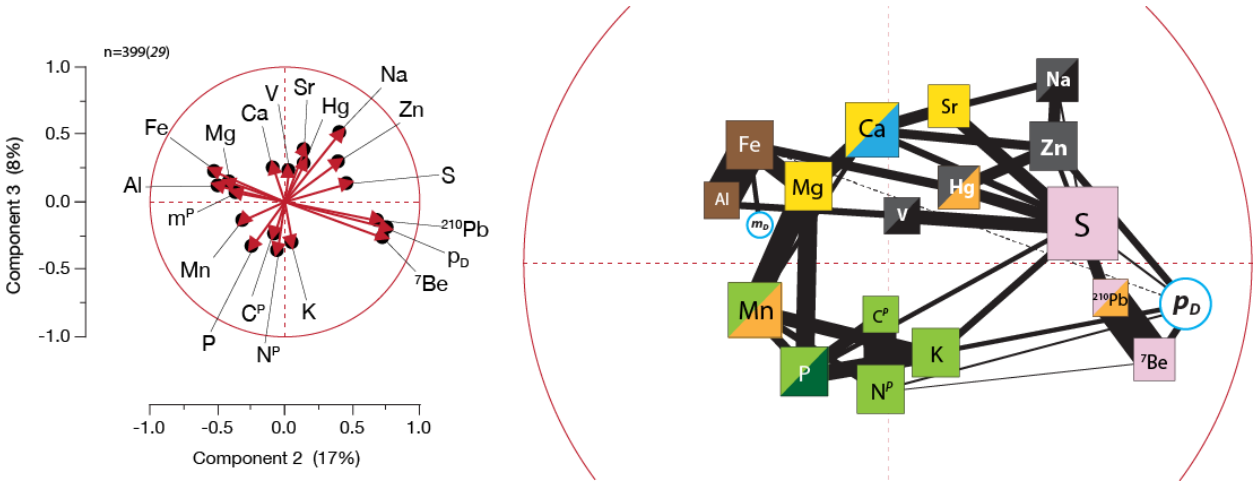

Figure 3: (a) Principle Component Analysis for fallout radionuclides (FRNs) and major/trace elements (MTEs) in bulk atmospheric deposition. (b) Correlation Network illustration for FRNs/MTEs based on multiple linear regression. Each independent correlation is represented by a connecting line (edge) and weighted by R^2. Dashed lines indicate anti-correlations. Sizes of variables (vertices) are weighted by the number of independent correlations. Variable colors represent assigned aerosol types as follows: secondary aerosol (pink), biogenic aerosol (green), anthropogenic aerosol (gray), soluble mineral aerosol (yellow), insoluble lithogenic aerosol (brown). Split colors indicate multivariate seasonality for winter (black), spring (blue), summer (green), autumn (orange). Precipitation depth (p_D) and mass deposition (m_D) were included in the analysis and are shown as circles.

4.3. FRN aerosol populations are discriminated by ^{7}Be: ^{210}Pb ratios

4.3.1. ^{7}Be: ^{210}Pb ratios scale with precipitation depth: While depositional fluxes of ^{7}Be and ^{210}Pb were strongly correlated through their mutual control by p_D, we found that p_D also explained a large amount of variance in ^{7}Be:^{210}Pb

ratios (Figure 4). Here we grouped samples by the following compartments: ambient aerosol (PM10), dry deposition, trace p_D (<3mm), moderate p_D (3-15 mm), and high p_D (>15 mm) [$R_a{}^2$=0.24, $F(4,564)$=41.6, p<0.0001]. The mean ^{7}Be:^{210}Pb ratio in each group was significantly different than all others [p<0.05] (Figure 4b). Importantly, each dry or wet compartment in bulk deposition was also different than ambient PM10 aerosols [p<0.05], an indication that bulk deposition must include aerosol sources, populations, depositional mechanisms or processes that are not represented by PM10 aerosol. We address different contributing mechanisms in *Section 4.6*.

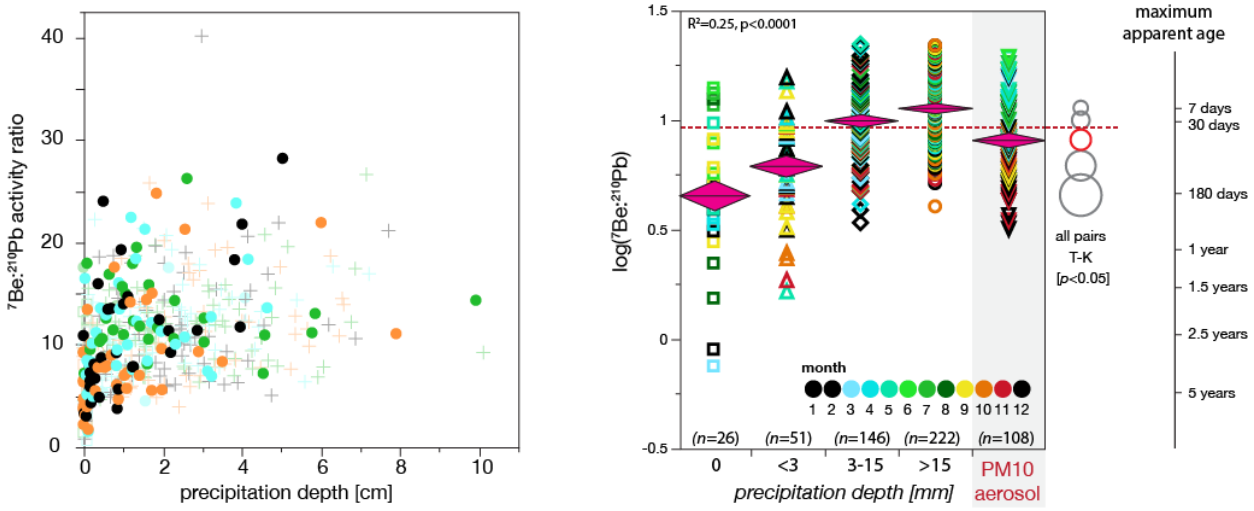

Figure 4: (a) ^{7}Be:^{210}Pb activity ratio versus precipitation depth (p_D). Circles show single-storm and crosses multi-storm collections. Symbols are color-coded season, winter=black, spring=blue, summer=green, autumn=orange. (b) ^{7}Be:^{210}Pb categorized by depositional compartments according to p_D. These include bulk dry deposition (mean =4.5 ±0.4 1SE, n=27), <3 mm (trace p_D) (6.6 ±0.4, n=51), 3-15 mm (10.0 ±0.4, n=146), >15 mm (11.8 ±0.3, n=222), and PM10 aerosol (8.2 ±0.3, n=108). FRN ratios can provide an estimate of maximum apparent aerosol age assuming an open-system accumulation model and, here, and initial ^{7}Be:^{210}Pb equal to the flux-weighted mean =10.8. Apparent age represents total aerosol lifetime in production, deposition, resuspension; the estimate is a maximum, assuming a constant rate of FRN accumulation (see *Section 5.2*; *Landis et al. 2014*).

4.3.2. ^{7}Be: ^{210}Pb ratios show meteorological dependence: Independent of the separation provided by p_D, an isotope mixing plot of ^{7}Be vs ^{7}Be:^{210}Pb revealed three distinct groupings among bulk collections. These cumulatively explained the largest proportion of variance yet [$R_a{}^2$=0.42, n=461(*3*), F(*2,459*)=174, p<0.0001] (Figure 5). We used discriminant analysis to define empirical groups in the isotope mixing plot, describing them as depleted in ^{210}Pb (D), enriched in both ^{7}Be and ^{210}Pb (E), or otherwise normal (N). Independence of this

grouping from p_D suggests a reliance on meteorological control (*Section 4.4*).

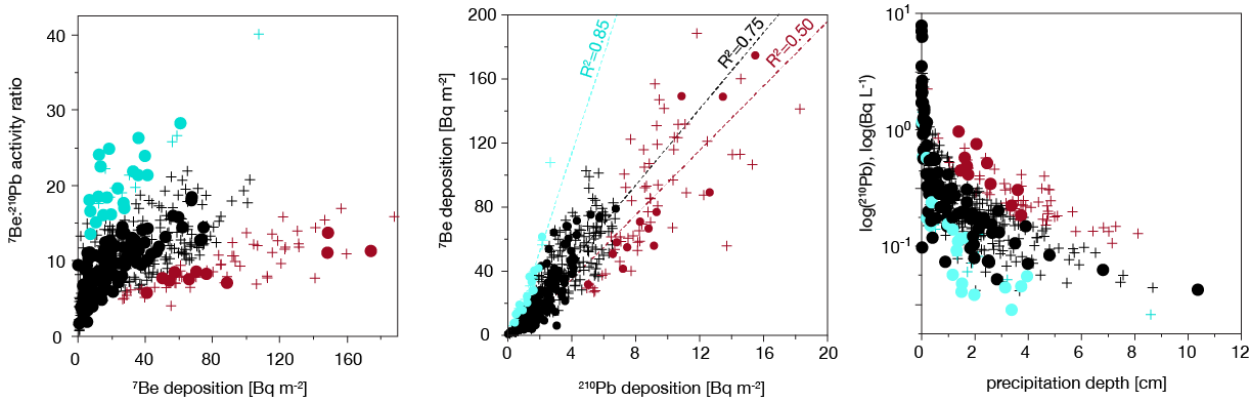

Figure 5: (a) ^{7}Be-^{210}Pb mixing diagram for bulk atmospheric deposition. Samples fall in three empirical groups, normal (black), ^{210}Pb-depleted (aquamarine), ^{7}Be-and-^{210}Pb-enriched (red). Symbols are circles for single-storm and crosses for multi-storm collections. (b) within-group linear correlations for ^{7}Be vs. ^{210}Pb deposition. (c) ^{210}Pb concentration versus precipitation depth for groups.

4.3.3. ^{7}Be: ^{210}Pb ratios reveal seasonality and long-term trends: We observed a small increase in ^{7}Be:^{210}Pb ratios following the long-term decline in ^{210}Pb deposition [Figure 6; 3.4 ±0.8% y^{-1}, p<0.0001]. We also observed minor seasonal variation in ratios, with summer months recording higher and fall months lower ones [R_a^2=0.031, F(11,441)=2.32, p<0.0088; Figure 6b]. The annual timing of these shifts was irregular, however, with no detectable periodicity in the timeseries [Kappa p=0.73, Bartlett's K-S = 0.091]. We discuss underlying seasonality in FRN and S deposition in *Section 4.5*.

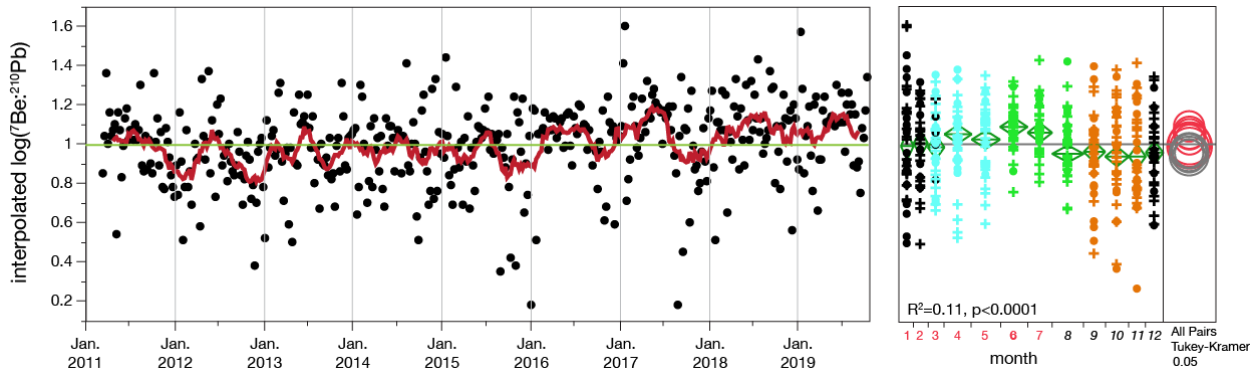

Figure 6: (a) timeseries for ^{7}Be:^{210}Pb ratios of weekly bulk deposition collections (n=461; log-transformed and interpolated to uniform 7-day frequency). A red line shows the centered 12-week running average. A green line indicates the

record average. (b) ANOVA with flux-weighted ^{7}Be:^{210}Pb ratios by month. Symbols are colored by season for winter (black), spring (blue), summer (green), autumn (orange). Circles show single-storm and crosses multi-storm samples.

4.4. ^{7}Be:^{210}Pb ratios are influenced by meteorological controls

To describe meteorological influences on ^{7}Be:^{210}Pb ratios of bulk deposition, we evaluated 73 collections that captured individual storm events with greater than 1 cm of precipitation. Similar to *Huang et al.* (*2018*), we combined Hybrid Single Particle Lagrangian Integrated Trajectory Model back-trajectories (HYSPLIT, *Stein et al. 2015*) and National Weather Service daily weather maps (*NOAA*) to classify storms in this subset as continental mid-latitude cyclones (H), marine mid-latitude cyclones (L), or frontal systems (f) (Figure 7). The E events were predominantly derived from continental trajectories, with 50% related to H cyclones and all (100%) associated with cold fronts. In contrast, D events showed marine trajectories, and 83% were related to L cyclones. Nearly all D events (92%) were associated with warm fronts. In correspondence analysis, L storms correspond to D events, H storms to E events, and f storms with N events (Figure SI 5; R^2=0.29, $X^2(4)$=36, p<0.0001). This confirms a meteorological basis for our *E-N-D* categorization.

To extend the *E-N-D* classification to the full dataset for subsequent analyses, we again used discriminant analysis to create new multi-storm categories E^m, N^m, and D^m based on the corresponding single-storm definitions and mixing plot. The categorization of single-storm vs. multi-storm is an approximation for the time-fraction of active precipitation during each collection period (i.e., single-

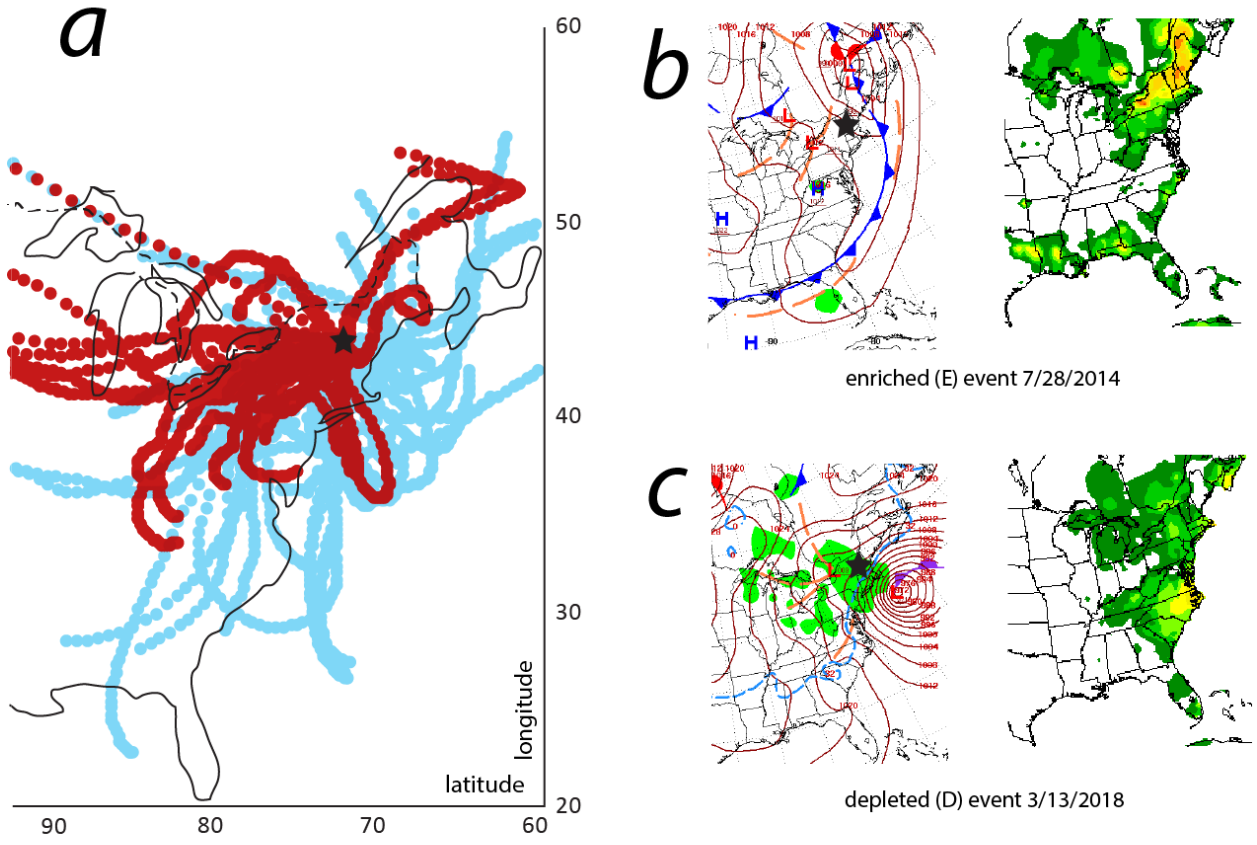

Figure 7: (a) map of eastern USA with composite 72-hour HYSPLIT back-trajectories for FRN enriched (E) storms (red; n=10) and depleted (D) storms (blue, n=13). The Hanover, NH study site is marked with a star. (b) National Weather Service (NOAA) daily weather and 24-hour precipitation maps for an E-storm characterized by on-shore low and cold front passing northwest of Hanover. (c) a D-storm with characteristic off-shore low and warm front passing southeast of Hanover.

events have small fractions of time with active precipitation, multi-events with greater fractions of time with active precipitation). Differences between single- and multi-storm categories should relate to rates of aerosol depletion and recharge during and between storms. Details are provided in *Supporting Information*.

We evaluated bias in FRN/MTE deposition between single-storm and multi-storm collections as follows, first normalizing for precipitation depth by regressing FRN/MTE concentrations against p_D (since the multi-storm collections have

higher precipitation totals). For each FRN/MTE we tested whether residuals for each of the E^m-N^m-D^m categories were different than the corresponding *E*-*N*-*D* single-storm with these hypotheses: $N^m \neq N$, $E^m \neq E$, $D^m \neq D$. Just one difference was significant: for a given precipitation depth, ^{7}Be in multi-storm N^m collections showed 23% higher concentrations than single-storm *N* collections [p=0.0097]. By comparison, neither the other secondary aerosols ^{210}Pb [p=0.20] or S [p=0.80], nor any other MTEs followed this pattern (Table 3). This implies that ^{7}Be is recharged more efficiently between storms.

We subsequently consolidated all single- and multi-collections into the three *E*-*N*-*D* storm types, where the combined *E*-type accounted for 21% of total collections (n=97), *N*-type accounted for 66% (n=306), and *D*-type accounted for 12% (n=57). We note that while the *E*-*N*-*D* storm types were defined using ^{7}Be and ^{210}Pb, each was distinguished by unique MTE composition as well [MANOVA p<0.0001; *Supporting Information*).

We interpreted *E*-type storms as strong convective events of continental origin (similar to the "Alberta clipper" originating from Alberta or Alaska Lows). They were biased to summer [$X^2(4)$= 10.2, p<0.05; Figure SI 5], typically driven by cold fronts, and had higher rainfall totals than either *D*- or *N*-type events [p<0.05]. Even when normalized for p_D, fluxes of ^{7}Be,^{210}Pb and S, and all other FRNs/MTEs were enriched in *E* events relative to those in both *N* and *D* events [p<0.05; Table 3]. Co-enrichment of ^{7}Be, ^{210}Pb and terrestrial aerosols is consistent with strong convection, lateral entrainment and vertical mixing of ascending boundary layer and descending upper atmospheric air contributing to large aerosol fluxes, irrespective of aerosol production altitude (*Su et al. 2003*, *McNeary and Baskaran 2003*, *Chen et al. 2016, Du et al. 2015*).

In contrast, *D*-type events were related to low-latitude, low pressure systems with marine moisture sources moving up the eastern US seaboard ("nor'easters" developed from Gulf or Hatteras Lows). These events did not have significant seasonality. *D*-type events were depleted due to negligible ^{210}Pb production in the oceans (*Baskaran 2011*, *Renfro et al. 2013*, *Du et al. 2015*). Likewise, the *D* events were also depleted in S and mineral elements Fe, Al, Mg, Ca [p<0.05]. However, they were not depleted in ^{7}Be or either biogenic or anthropogenic elements including N^P, C^P, P, K, Hg, Na and Zn [p>0.05]. The combination of ^{7}Be and Na with biogenic elements is consistent with a marine aerosol source (e.g., *Sanchez et al. 2021*).

4.5. FRNs and S exhibit both shared and uniqu seasonal controls

We evaluated two views of seasonality in FRN/MTE deposition, first the observed patterns in bulk depositional fluxes, hereafter called objective seasonality, since these bear ecological and geochemical consequences. We also described seasonality in FRNs/MTEs that was independent of patterns in precipitation or dustiness, which we call intrinsic seasonality, since these reflect behaviors of aerosol types or individual FRNs/MTEs. These two views of seasonality are compared in Table 2.

Observed fluxes of ^{7}Be, ^{210}Pb and S each showed summer maxima that were significantly higher than annual means: ^{210}Pb (+42%) >^{7}Be (+41%) >S (+35%). Seasonality of MTEs is shown in Table 2. The magnitudes of seasonal differences for ^{7}Be, ^{210}Pb and S were large despite explaining small proportions of variances, underscoring the importance of a large dataset for detecting these effects – the seasonal signal is obscured since p_D is the largest source of variance through the washout-rainout transition (e.g., *Dibb 1989*, *Kim et al. 2000;* Figure 5c). Moreover, because we have already seen that p_D is a primary control on flux of the secondary aerosols, we anticipated that some seasonality is a consequence of this, as well, since summer p_D was 33% greater than the annual mean. Similarly, the MTEs most strongly correlated with m_D (Mg, Fe, Al, Ca, Mn) showed spring maxima *ca.* 50% higher than annual means due to seasonality in dustiness (Table 3).

To describe intrinsic seasonality, which is independent of precipitation or dust, we used multiple regressions to model normalized FRN/MTE concentrations ($_i$) with season, p_D, m_D and storm type as explanators. $_i$ implicitly compares annual distributions of deposition and precipitation and is calculated as the quotient $_i = _i/ _P$, where $_i$ is the fraction of FRN/MTE annual flux and $_P$ is the fraction of annual precipitation per each collection (*Baskaran 1995, Mohan et al. 2019*). Multiple regressions revealed an intrinsic summer bias in each of ^{7}Be (+15% over mean), S (+10%), ^{210}Pb (+8%). Summer maxima of biogenic elements were even higher than their objective effects: P (+93%) >N^{P} (+67%) >K (+53%) >C^{P} (+38%). Mineral aerosols maintained their spring enrichments, Mg (+36%) >Fe (+25%) >Al (+26%). Three metals showed strongest enrichments in autumn, Hg (+39) >Mn (+36%) >V (25%), and two in winter: Na (+97%) >Zn (+11%). Multiple regression results for all explanators are summarized in Table SI 1.

4.6. Depositional mechanisms: FRN and S deposition is apportioned by dry, washout, and rainout processes

4.6.1. Dry deposition: We estimated dry contributions to total annual deposition by assuming that dry processes are active to the same degree during all days, irrespective of precipitation. Multiplying the daily dry depositional rate by number of days in the year, we estimated the annual contribution of dry deposition for ^{7}Be to be 3.8 ±0.5% (mean ±SE), significantly lower than for ^{210}Pb [10.9 ±1.2%; $t(37)$=-5.6, p<0.0001]. Both are consistent with other measures from around the globe (Figure SI 6). Our estimate of dry contribution to total S deposition is much higher than for the FRNs (46 ±5%). This was expected due to the efficient dry deposition of SO_2 and was moreover consistent with modeled estimates for the eastern US (38%; *Baumgardner et al. 2002, Nopmongcol et al. 2019*). The assumption of a constant daily rate may overestimate dry deposition since we extrapolate to periods when wet processes prevail. Measured annual wet and dry fluxes for FRNs and MTEs are summarized in Table 1.

We note that while the relative dry contribution to annual deposition for ^{7}Be is a factor of 2.9 less than for ^{210}Pb, their equivalent dry depositional velocities (v_D) were not significantly different: 127 ±24 m d^{-1} for ^{7}Be (mean ±SE, n=7

collections or 49 days) versus 97 ±14 m d^{-1} for ^{210}Pb. v_D was calculated as bulk dry flux [Bq m^{-2} d^{-1}] divided by concentration in ambient air [Bq m^{-3}]. Indistinguishable v_D for ^{7}Be and ^{210}Pb indicates that the process of dry deposition influences ^{7}Be and ^{210}Pb similarly. Different dry contributions to annual flux are instead attributable to different contributions by wet deposition. This is evident among global sites, where the dry contribution to annual bulk deposition is inversely related to total annual precipitation for both ^{7}Be [R^2=0.84, p=0.003, n=7] and ^{210}Pb [R^2=0.84, p=0.003, n=7] (Figure SI 6).

4.6.2. Wet deposition by washout and rainout: A transition from washout to rainout of aerosols during storm events produces a characteristic exponential decline in aerosol concentrations with increasing precipitation. We compare ^{7}Be, ^{210}Pb and S in Figure 8. There, regression slopes for normalized concentration versus normalized p_D reflect the degree of mixing between dry+washout and rainout aerosols. A slope of -1 would indicate pure dilution of a dry+washout aerosol source by increasing p_D, i.e., condensation of pure water with no rainout aerosol. A slope of 0 would indicate a pure rainout aerosol source with no below-cloud contributions from washout (*Supporting Information*). Each of the slopes for ^{7}Be, ^{210}Pb and S are significantly different than -1 and also each from another, confirming that each is influenced by a unique combination of dry+washout/rainout sources. Scatter about the best fit reflects inter-storm variations due to meteorology, seasonality, etc.

To quantify average per-event contributions of dry, washout and rainout processes to FRN deposition we applied the model of *Ishikawa* (*1995*) and *Caillet et al.* (*2001*), with an assumption that inter-storm variations in p_D recapitulate the intra-storm evolution of FRN fluxes:

$C_i = \frac{(w_0^i + d_0^i)}{p_D \bullet 10} + r^i$ Eq. 5

Here C_i is the measured concentration of each FRN or MTE in precipitation, w_0 is washout and d_0 is dry deposition represented as fixed areal fluxes [Bq m^{-2} or mg m^{-2} per event], p_D is precipitation [cm] and r represents concentration in condensation nuclei [Bq L^{-1}or mg L^{-1}]. A factor of 10 converts areal deposition [Bq m^{-2}] to concentration [Bq L^{-1}]. Independence of w_0 from p_D is an oversimplification, i.e., washout is not deposited instantaneously and requires some finite volume of p_D to be fully removed from suspension. From our data it appears that 3 mm of precipitation is sufficient to scavenge most of the washout fraction. The washout-rainout transition can alternatively be modeled as a continuous process using a power law, $C_i = \alpha_i {p_D}^{\beta_i}$, and with β representing a scavenging efficiency (*Sportisse 2007*). In comparing washout-rainout and power law models, we found that they yield comparable goodness-of-fits and, across all FRNs/MTEs, the ratio r_0/w_0 was linearly related to 10^{β} ($R_a{}^2$=0.98). We show both models in Figure 8.

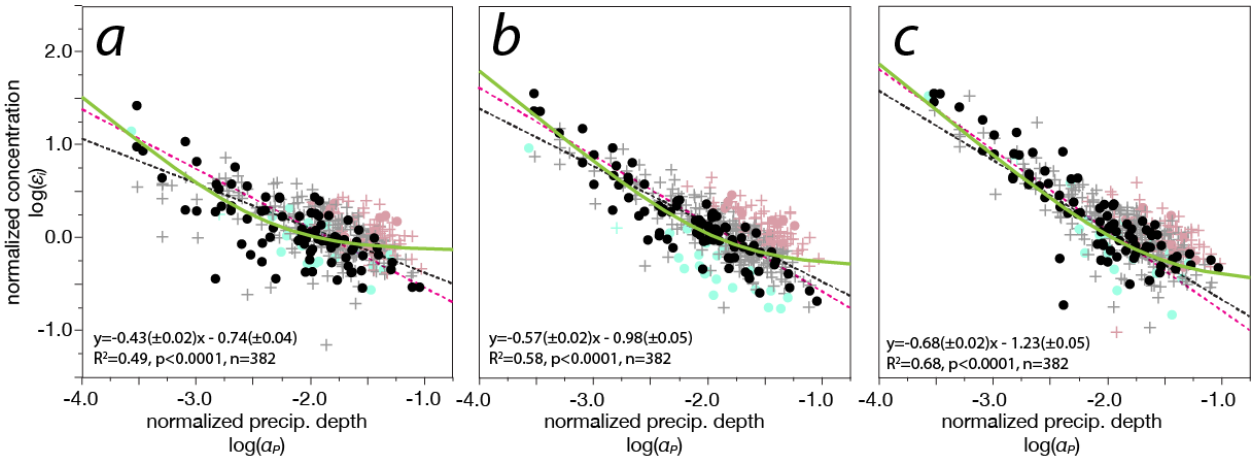

Figure 8: normalized concentrations ($_i$) versus normalized precipitation ($_P$) for ^{7}Be, ^{210}Pb and S. See *Section 4.5* for explanations of $_i$ and $_P$. A slope greater than -1 indicates mixing of different aerosol populations through the washout-rainout transition. Circles show single-storm and crosses multi-storm collections. Symbols are colored coded by storm type. Regressions were made only to normal-type (N) storms (black circles, bold). Green curves show washout-rainout models, black dashed lines show power law models, and pink dashed lines show linear orthogonal fits. Regression equations are shown for orthogonal fits.

The advantage of the *Ishikawa* model is that it allows a mass-balance apportionment of deposition to discrete, interpretable and physical mechanisms. To apportion bulk flux using Eq. 5 we used only the *N*-type single-events from the "A" collector (n=87) and omitted *E* and *D*-type events to avoid meteorological biases (apparent in Figure 8b). The sum (w_0 + d_0) was obtained by least-squares fitting, and w_0 was then calculated by subtracting measured dry fluxes (d_0). Because the rainout flux scales with p_{D} we calculated it by mass balance with $(d_0 + w_0 + r_0)/T_0 = 1$, and total fluxes ($T_0$) equal to the observed mean event flux (corresponding to p_D ~1.2 cm). Thus, these results apportion areal deposition on a per-event basis (in contrast to flux-weighted annual totals in Table 1):

^{7}Be: d_0 (5%) + w_0 (14%) +r_0 (82%) =100%

^{210}Pb: d_0 (14%) + w_0 (28%) + r_0 (58%) =100%

soluble S: d_0 (56%) + w_0 (15%) + r_0 (29%) =100%

Through this apportionment we established that the characteristic depositional processes for ^{7}Be, ^{210}Pb and S are quite different. ^{7}Be had minor contributions from dry deposition, and in wet deposition was dominated by rainout over washout by a factor of 6 (r_0/w_0 =5.9). ^{210}Pb deposition had significant contributions from both dry and wet processes, but wet deposition was divided between

washout and rainout (r_0/w_0 =2.0). Sulfur deposition was dominated by dry deposition (attributable to gaseous SO_2), while the importance of washout was intermediate between that of ^{7}Be and ^{210}Pb (r_0/w_0 =2).

Importantly, the modeled ^{7}Be:^{210}Pb ratio of washout (=5.5 ±0.9) is different than ambient PM10 aerosol (=8.2 ±0.3; Figure 4) and is instead more comparable to measured bulk dry deposition (^{7}Be:^{210}Pb =4.5 ±0.4, n=37). This suggests that washout and dry fractions may share common sources and aerosol characteristics. In contrast, the typical ^{7}Be:^{210}Pb ratio of rainout is higher by a factor of three (=16.0 ±1.1), about 50% higher than the flux-weighted mean (=10.8 ±0.3). Together these results re-emphasize the diversity of aerosol sources that contribute to FRN bulk deposition.

4.7. Integrating sources, processes, and chemistries in aerosol deposition

Separating the simultaneous influences of chemistry, meteorology and depositional mechanism controls described in *Sections 4.2 – 4.6* require a multivariate approach. Towards this, we reintroduce multiple regression. We have already used multiple regressions in *Section 4.4* to test *a priori* hypotheses about seasonality in FRN/MTE deposition – these are called the general models hereafter. We can use these general models to examine the importance of p_D, m_D and storm type to deposition of ^{7}Be, ^{210}Pb and S as described below, illustrated in Figures 9a to 9c, and summarized in Table SI 1.

We next exploit the normalizing effect of the ^{7}Be:^{210}Pb ratio and other MTE parameters to achieve better of specificity in the models, by next adding individual FRNs/MTEs as new explanators in the general models. This allows us to normalize effects that might be shared by FRNs/MTEs within their aerosol types, and thereby expose effects that we consider intrinsic to the individual FRN or MTE response variable. FRN/MTEs were added step-wise to each general model and explanators removed as their effects were superseded by stronger ones. For ^{7}Be we also included sunspot number as an explanator. These specific models are discussed below and illustrated in Figures 9d to 9f.

4.7.1. Multiple regression for ^{7}Be: For ^{7}Be deposition the general model was highly predictive [$R_a{}^2$=0.73], with p_D the strongest explanator [e^*=62%] and lesser effects from both storm type [7%] and seasonality [2%]. Effects of general factors on ^{7}Be are illustrated in Figure 9a, with bivariate correlations among explanators indicated with connecting lines. Adding FRNs/MTEs step-wise to the ^{7}Be general model yielded significant effects from both ^{210}Pb [e^*=62%] and N^P [e^*=1%] while improving the overall model prediction (R^2=0.92). Substitution of N^P with P yields a comparable result, providing strong evidence of an influence of biogenic aerosol on ^{7}Be deposition. Similarly, only when ^{7}Be was normalized by inclusion of ^{210}Pb in the model did a significant effect from sunspot number emerge [e^*=1%]. A final best fit is illustrated in Figure 9d.

In the final model ^{7}Be deposition correlated most strongly with ^{210}Pb but retained strong dependence on p_D [e^*=11%]. The predominance of ^{210}Pb over

p_D as an explanator underscores the importance of micrometeorological factors over precipitation alone in depositing FRNs, e.g., scavenging efficiencies related to precipitation rate or sizes of aerosols and raindrops. The additional dependence of ^{7}Be on p_D, independent of ^{210}Pb, reflects stronger roles of rainout and synoptic atmospheric recharge in ^{7}Be deposition through lateral and long-range transport (*Brattich et al. 2017*). Summer seasonality in ^{7}Be was largely incorporated through ^{210}Pb and N^P, but a small negative bias to autumn remained in the model [e^*=1%] with seasons ordered: summer^{A} >spring^{AB} > winter^{B} >autumn^{C} [p<0.05]. With addition of ^{210}Pb and N^P to the model, the storm-type effect on ^{7}Be deposition was strengthened [e^*=10%] but reversed in order as $D^{A} > N^{B} > E^{C}$. This result reflects a stronger control of these event definitions on ^{210}Pb than ^{7}Be, but we cannot rule out an enrichment of ^{7}Be in marine air. Correlation with N^P reflects, in part, shared summer

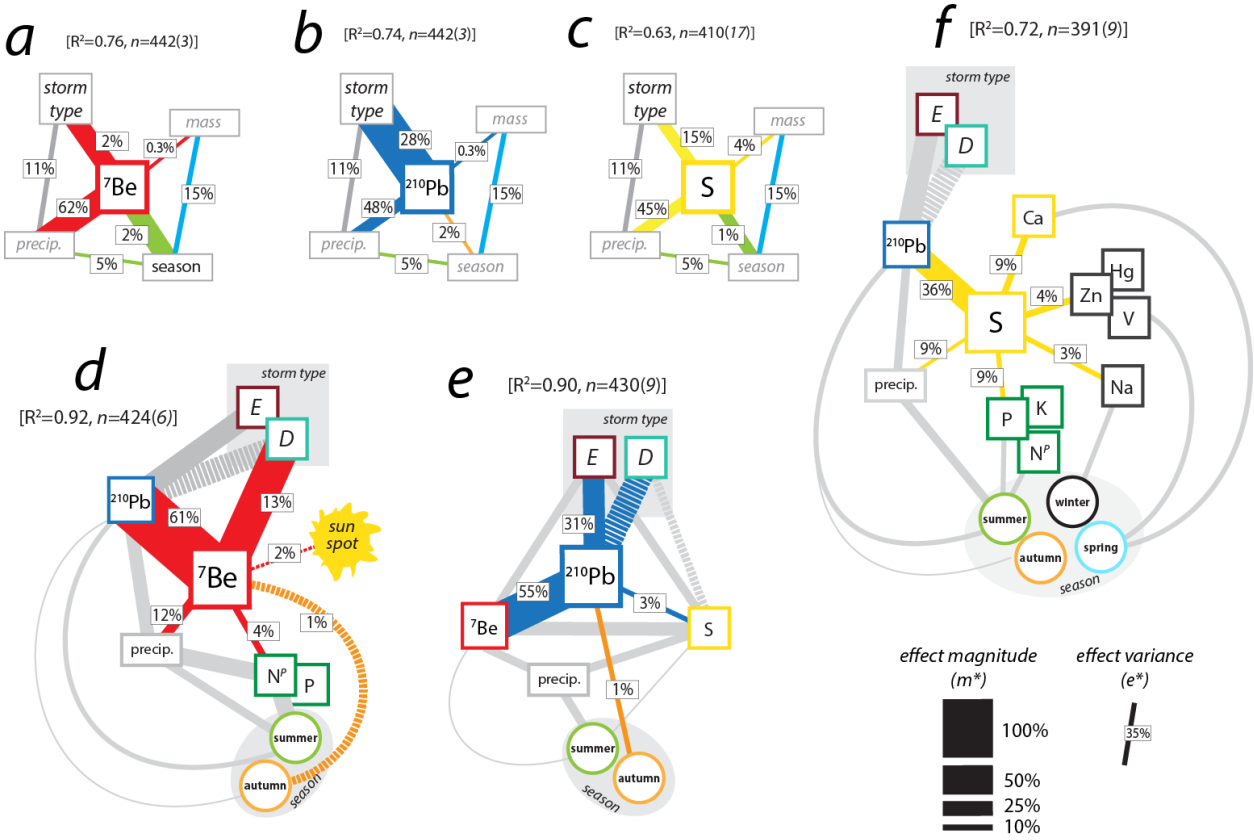

Figure 9: multiple regression correlation web for bulk deposition of ^{7}Be, ^{210}Pb and S. (a-c) general models included environmental variables precipitation depth (p_D), mass deposition (m_D), storm type and season as explanators. (d-f) specific models added FRNs and MTEs to each general model step-wise, with stronger explanators superceding and displacing weaker ones. In each model a central

response variable is connected by lines with significant independent explanators. Dashed lines indicate anti-correlations. Thickness of connecting lines is proportional to effect magnitude (change in response per doubling of explanator). Numbers report the proportion of response variance that is explained by the explanator.

seasonality, but may also be indicative of marine biogenic aerosol. Other similarities between ^{7}Be and N^{P} include strong dependence on p_D and abundance in *D*-type events.

4.7.2. Multiple regression for ^{210}Pb: The general model for ^{210}Pb explained 71% of variance [R_a^2=0.70] with strongest effects divided between p_D [e^*=36%] and storm type [e^*=35%] (Figure 9b). Adding ^{7}Be and S to the model explained an additional 17% of variance [R_a^2=0.88], while removing any influence of p_D [p=0.52]. In this case ^{7}Be became the strongest predictor of ^{210}Pb [e^*=63%] with storm type contributing an additional 25% and S a modest effect [2%]. With addition of ^{7}Be, p_D no longer exerted independent control on ^{210}Pb due to the lesser importance of the rainout mechanism on ^{210}Pb. The persistent control of storm type on ^{210}Pb deposition retained the ordering $E^{A} > N^{B} > D^{C}$ [p<0.05], reflecting strong, intrinsic source effects in ^{210}Pb deposition. *E*-type storms were enriched through strong convection and entrainment of low-altitude aerosols, and *D* storms were depleted as a longitudinal consequence of a marine moisture source and lack of ^{210}Pb production in seawater. The ^{210}Pb correlation with S could indicate a specific interaction such as formation of $PbSO_4$, some shared influence of dry processes in their deposition, commonalities in their atmospheric transport through low-altitude production (e.g., *Dibb et al. 1992*), or some combination of these. It is noteworthy that this correlation is independent of mutual long-term decline in S and substituting non-detrended S data into the model doubled the effect of S on ^{210}Pb deposition. We speculate that higher S concentrations in the atmosphere could increase the depositional efficiency of ^{210}Pb through either wet or dry processes, possibly through formation of insoluble $PbSO_4$. A final model for ^{210}Pb deposition is illustrated in Figure 9e.

4.7.3. Multiple regression for S: The general model for S deposition explained 56% of variance [R_a^2=0.56] (Figure 9c). The step-wise regression added significant correlations with each of ^{210}Pb, Ca, P, Zn, Na and p_D, collectively explaining an additional 16% of variance [R_a^2=0.72] (Figure 9f). ^{210}Pb superseded p_D to become the strongest explanator [e^*=36%]. Among MTEs, Ca was the single strongest explanator [10%], superseding m_D but also explaining a much larger portion of variance. Formation of $CaSO_4$ through neutralization of SO_4 could enhance scavenging of S from dry and wet deposition. Sulfate mineralization could also influence the behavior of ^{210}Pb as both Ca and Pb sulfates are commonly identified in aerosols (*Sakata et al. 2014, Sakata et al. 2017*). Among other MTEs, P and N^{P} had similar contributions [e^*=9%]. These reflect a bias towards biogenic over inorganic sources for S. Zn, Hg or V all contributed comparable effects [4%], each indicative of a combustion source

of S. Finally, Na contributed a small effect that could be indicative of seasalt [e^*=3%]. Storm-type controls on S deposition were expressed through ^{210}Pb. Yet, similar to ^{7}Be, a significant p_D effect persisted in the S multiple regression [e^*=9%], reflecting stronger rainout contributions for S than for ^{210}Pb. While there were no direct effects from seasonality in S deposition in this model, each of its covarying aerosol types has unique seasonal forcing. This implies that there are seasonal variations in S provenance and/or speciation, with inorganic S biased to spring, biogenic S to summer, and anthropogenic S to winter. A final, best-fit model for S deposition is shown in Figure 9f.

4.8. Assessing global controls on ^{7}Be:^{210}Pb ratios

Some of the controls on ^{7}Be:^{210}Pb we have described, such as scaling with p_D, the washout-rainout transition, storm tracks and convection, and synoptic recharge, have climatic implications and thus the potential to exert control on ^{7}Be:^{210}Pb depositional ratios at the global scale. Since compiled global data have not been evaluated from the perspective of ^{7}Be:^{210}Pb ratios, we present an analysis here based on the recent compilation of *Zhang et al.* (*2021*). Data sources are listed in *Methods*, and more details are provided in *Supporting Information*.

Best available data coverage for both ^{7}Be and ^{210}Pb data is biased geographically to two regions, North America/Western Europe (NAE) and Southeast/East Asia (SEA). These sites form coherent groups in ^{7}Be:^{210}Pb data as well [R^2=0.63, $F(1,75)$=131, p<0.0001]. Among NAE sites^{7}Be:^{210}Pb flux ratios increase strongly with p_D [R^2=0.63, p<0.0001] (Figure 10) due to its control on ^{7}Be flux [p<0.0001]. In comparison, we see no control of p_D on ^{7}Be:^{210}Pb ratios for SEA sites [R^2=-0.01, p=0.50]

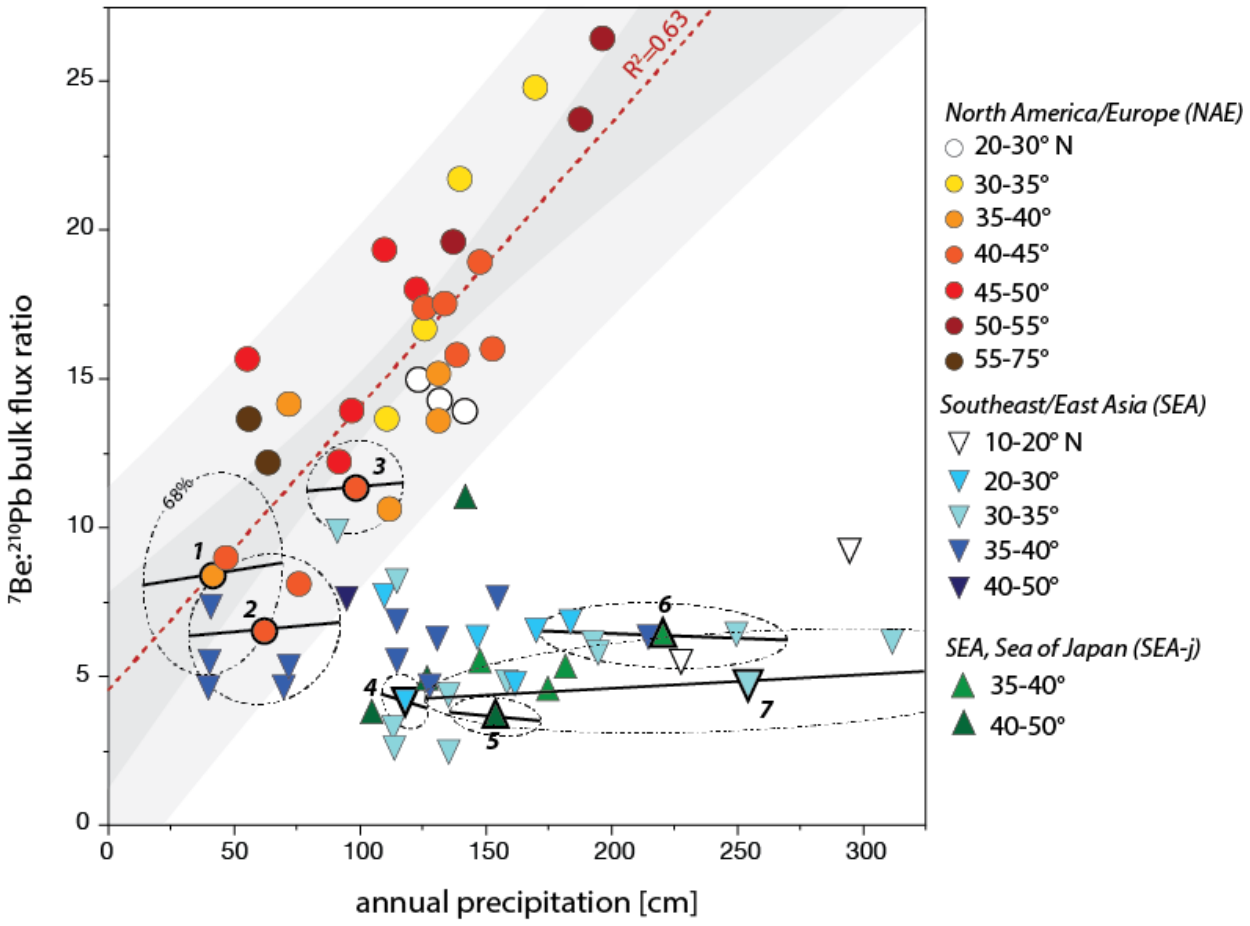

Figure 10: mean ^{7}Be:^{210}Pb activity ratio versus annual precipitation for global sites compiled by *Zhang et al.* (*2021*). Sites are grouped regionally with circles for North American/European sites (NAE) and triangles for Southeast/East Asian sites (SEA). Sites are color-coded by latitude within regions. Regressions and shaded confidence intervals are shown by region: NAE, ^{7}Be:^{210}Pb=4.5(±1.6) + 0.095(±0.013)*p_D; SAE, ^{7}Be:^{210}Pb=5.4(±0.7) + 0.002(±0.004)*p_D; SAE-j, ^{7}Be:^{210}Pb=3.7(±4.6) + 0.012(±0.028)*p_D. For sites with multi-year records, 1-sigma confidence ellipses and linear fits display interannual variation (none significant at p<0.05): (1) Malaga (n=11, *Duenas et al. 2017*); (2) Monaco (n=13, *Pham et al. 2013*); (3) Hanover (n=9, *Landis et al. this manuscript*); (4) Shanghai (n=7, *Du et al. 2015*); (5) Rokkasho (n=5, *Akata et al. 2008*); (6) Tatsunokuchi (n=12, *Yamamoto et al. 2006*); (7) Taipei (n=17, *Lee et al. 2015*).

This striking difference between the NAE and SEA regions may be explained by differences in how effectively high-altitude, high-latitude, ^{7,10}Be-enriched air

is accessed by dominant weather patterns. Coastal and inland NAE sites alike have year-round influence from high-latitude, high-pressure systems. There, ^{7,10}Be deposition is enhanced by what we have called synoptic atmospheric recharge, which is advective (additive) funneling of airmass and aerosol through lateral transport along the polar jet in mid-latitude storm belts (e.g., *Field et al. 2006*). Access to the stratospheric ^{7,10}Be source is promoted where vertical mixing is high and cyclone formation is preferred (*Brattich et al. 2017*). As a result, ^{7,10}Be deposition increases strongly with p_D [14.5 ±3.1 Bq m^{-2} y^{-1} cm^{-1}; $R_a{}^2$=0.41, p<0.0001, n=31], while ^{210}Pb does not [p=0.88].

For SEA sites, precipitation is controlled by the persistent Asian Low, shifting ITCZ, low-latitude storm tracks and summer/winter monsoon. Despite some sites being at latitudes comparable to NAE sites, these are effectively isolated from mid-latitude cyclone activity and strong vertical mixing that accesses ^{7,10}Be aloft. Instead, ^{7,10}Be deposition reflects a dilutative effect whereby a finite burden of FRN aerosols is diluted by increasing rainfall (*Willenbring and von Blackenburg 2010*). ^{7}Be deposition increases only modestly with p_D, at rate five times lower than that of NAE sites [3.4 ±1.2 Bq m^{-2} y^{-1} cm^{-1}; $R_a{}^2$=0.18, p=0.008, n=32)]. ^{210}Pb again does not scale with p_D [p=0.57]. While seasonal shifts in aerosol source do occur, for example, the winter monsoon can deliver ^{210}Pb-enriched air from the Asian mainland, on an annual basis ^{7}Be and ^{210}Pb are influenced similarly by dominant processes in the SEA region. The ^{7}Be:^{210}Pb ratio is surprisingly invariant.

Both strong convection (*Su et al. 2003*) and orographic effects (*Yamamoto et al. 2006; Supporting Information*) can drive extraordinarily high FRN fluxes in the SEA region, yet both ^{7}Be and ^{210}Pb are influenced similarly. Sites on the Sea of Japan (SEA-j) are a case in point. Unlike other SEA sites, these northern-most ones are strongly influenced by continental storm tracks via Asian continental outflow and winter monsoon. Fluxes of ^{7}Be and ^{210}Pb alike at SEA-j sites are amplified by orographic uplift across the Japanese mainland, approaching extraordinary levels of 5000 Bq m^{-2} y^{-1} for ^{7}Be and 800 for Bq m^{-2} y^{-1} for ^{210}Pb. Nonetheless, both FRNs scale with p_D proportionately, and their ^{7}Be:^{210}Pb ratios are indistinguishable from other, southerly sites in the SEA region where fluxes are much lower [p=0.85].

Curiously, while p_D is a primary control on ^{7}Be:^{210}Pb ratios at the event scale (*Sections4.4, 4.6*), none of the multi-year records for either NAE or SEA regions show a dependence of ^{7}Be:^{210}Pb on annual p_D (Figure 10; *Supporting Information*).

. *Conclusions*

5.1. Seasonal influences in bulk deposition of ^{7}Be, ^{210}Pb and S

^{7}Be, ^{210}Pb and S all show highest depositional totals in summer. This could be viewed as a coincidence of their individual production sources strengthening in warm seasons (stratospheric intrusion and Rn emanation, respectively; *Caillet*

et al. 2001). But when also coupled with a summer maximum in S (*Section 4.5*), the coincidence seems more likely to reflect processes shared among secondary aerosols. These might include (1) strong convective mixing, simultaneously drawing ^{7}Be down from the upper atmosphere and both ^{210}Pb and S upwards (*Feeley et al. 1989*, *Dibb et al. 2003*, *McNeary and Baskaran 2003*). This process is consistent with the simultaneous enrichment all FRNs/MTEs in convective storms (*Section 4.4*). We should also consider (2) the temperature-dependence of aerosol abundance and nucleation events that spawn high aerosol densities (*Tunved et al. 2003*), which may in turn enhance the scavenging of secondary aerosols during spring and summer. Finally, (3) higher scavenging efficiencies associated with more intense rainfall could also enhance deposition of secondary aerosols (*Andronache 2003, Xu et al. 2019*), which could also contribute to the relative enrichments of ^{7}Be, ^{210}Pb and S in convective storms.

We were also able to detect important differences in FRN seasonalities by using multiple regression to control for micrometeorological commonalities shared by ^{7}Be and ^{210}Pb. A significant summer excess in ^{7}Be deposition over ^{210}Pb explained 1% of total variance but with a corresponding seasonal increase of 9% over the annual mean. The timing of this bias is broadly consistent with stratosphere-troposphere exchange (STE), a primary seasonal control on ^{7}Be aerosol concentrations in the mid-latitudes that drives increasing ^{7}Be:^{210}Pb ratios (*Feeley et al. 1989*, *Lee et al. 2007*). The stratosphere is an extreme potential source of cosmogenic ^{7,10}Be, representing >50% of total ^{7}Be and ^{10}Be production (*Masarik and Beer 1999*) but »90% of standing inventories due to the much longer residence time of stratospheric versus boundary layer aerosols (*Delaguay et al. 2015*).

FRN seasonalities also differed in an autumn ^{7}Be deficit of 11% relative to ^{210}Pb. This could reflect an antipode to STE, with cool weather, high boundary layer stability and low vertical mixing insulating stratospheric influence and thereby diminishing ^{7}Be source strength (e.g., *Lee et al. 2007*). Alternatively, the difference could reflect higher ^{210}Pb deposition. Other notable autumn effects in support of the latter interpretation include enhanced deposition of Mn, Hg, and V. Both ^{210}Pb (*Landis et al. 2014*) and atmospherically-derived metals including Hg accumulate in vegetation through summer months to such an extent that autumn leaf fall constitutes the predominant flux to terrestrial ecosystems (*Rea et al. 2002, Landre et al. 2010*). Contemporaneous increases in the bulk deposition of ^{210}Pb and other metals could derive from the production or resuspension of biogenic dust (*Kinase et al. 2013*), debris and associated metals. ^{7}Be:^{210}Pb ratios of this fraction would be low due to the short half-life of ^{7}Be.

5.2. Resuspension, recycling and particle aging in FRN deposition

The resuspension and recycling of aerosols is widely recognized in biogeochemical cycles of pollutants, MTEs and FRNs alike, but quantifying and characterizing this fraction remains a challenge. The highly-traceable radioactive aerosols generated in nuclear bomb testing and industrial accidents show that aerosols

remain in recirculation at the earth surface for years following deposition (e.g., *Kinase et al. 2018*) at a rates of 1-10% of total deposited amount (*Anspaugh et al. 2002*, *Vincent et al. 2019*). Isotopic measurements of stable Pb and ^{210}Pb reveal that legacy anthropogenic Pb from gasoline combustion persists in the surface environment several decades after its banning (*Yang and Appleby 2016, Farmer et al. 2007*). For other MTEs, resuspension is thought to contribute to excesses of measured over modeled dry deposition by as much as a factor of two (*Saylor et al. 2019*).

The difficulty in quantifying a recycled aerosol fraction lies in finding a tracer or index that distinguishes it from novel deposition. Recycled contributions to ^{210}Pb and ^{10}Be mass balances are typically estimated by indexing them to dust concentrations in bulk deposition. By this approach the recycled fraction of ^{10}Be deposition could be as much as 10-35% of measured ^{10}Be flux (*Brown et al. 1989*, *Monaghan et al. 1989*, *Ouimet et al. 2015*, *Graham et al. 2003*, *Graly et al. 2011*), or as little as 1-2% (*Dixon et al. 2018*). Comparable estimates of recycled ^{210}Pb are low, just 0.5% of annual deposition based on indexing to m_D or lithogenic MTEs such as ^{238}U (*Joshi and Mahadeavan 1968, Tokeida et al. 1996,* respectively). The variability in these estimates reflects, in part, uncertain assumptions about dust provenance and its characteristic FRN concentrations.

Here, despite very many measurements, we found no significant correlations of ^{210}Pb flux with m_D or MTEs such as Fe, Al or Ca that would unambiguously indicate a recycled fraction. Alternatively, correlations of ^{7}Be with N or P, and ^{210}Pb with S, could include recycled biogenic aerosols but more work will be required to understand these associations. Nonetheless, lower ^{7}Be:^{210}Pb ratios in both dry and washout deposition are conclusive evidence of an aerosol population that is distinct from PM10 aerosol. These lower ratios reflect contributions of an older, recycled aerosol population, enriched in ^{210}Pb due to its longer half-life. Instead of m_D or other elemental indices, here we indexed recycled ^{210}Pb to particulate carbon (C^P) since our local dust sources with highest concentrations of atmospheric ^{210}Pb are natural leaf litter (up to 100 Bq kg^{-1}) and organic-rich surface soils (up to 1500 Bq kg^{-1}). Estimated from these sources, the contribution of recycled ^{210}Pb to annual flux falls in the range of 0.2-5% as an uppermost limit. This is substantially lower than estimated from steady-state soils inventories which suggested a ^{210}Pb excess of 13% in bulk deposition. However, the soil mass balance approach is plagued by both analytical and geochemical uncertainties of the same order and we suggest that the indexing approach is like to be more reliable (*Yamamoto et al. 1998*; *Supporting Information*).

FRN isotopic systems provide another perspective into aerosol resuspension since their differing half-lives allow estimation of the timeframe over which the FRNs are recirculated. The short-lived daughters of ^{210}Pb in ambient aerosol are best known, ^{210}Bi (half-life 5.0 days) and ^{210}Po (half-life 138 days) (*Baskaran 2011*, *Dlugosz-Lisiecka and Bem 2012*). Whereas the ^{210}Bi:^{210}Pb chronometer yields accepted ages of 8 to 14 days for boundary layer PM2.5, the longer-lived ^{210}Po:^{210}Pb is often biased older with ages of 100-500 days for PM10 (*Marley*

et al. Aerosol Sci. Tech. 2000). In this case ^{210}Bi records aerosol condensation and coagulation, while the longer-lived ^{210}Po records subsequent resuspension and recycling (*Poet et al. 1972*, *Marley et al. 2000*, *Baskaran 2011*).

We can similarly estimate the age of recycled aerosols using ^{7}Be:^{210}Pb ratios, provided these assumptions (*Landis et al. 2014*): that the aerosols have an initial ^{7}Be:^{210}Pb ratio equal to that of flux-weighted precipitation (=10.8, see also *Landis et al. in review*), that FRNs accumulate in aerosols at constant rate and are lost only through radioactive decay (open-system model), and that that there is no fractionation between the FRNs. In this case the dry-deposited particles have a mean time in atmospheric transport, deposition and resuspension of about 180 days (Figure 4). For frame of reference, ^{7}Be:^{210}Pb ratios of our putative organic dust sources are 0.5 – 1.5 for leaf litter and 0.2 – 0.3 for forest topsoil, with corresponding ages of 1-1.5 years and 10-12 years, respectively (estimated using our Linked Radionuclide aCcumulation model (LRC), *Landis et al. 2016*).

Our dry deposition ages are identical to those that we compiled from global ^{7}Be:^{210}Pb ratios of dry deposition (4.4 ±0.5, mean ±SD, n=8;) and annual flux totals (Figure SI6). These equate to an age of 200 ±32 days using the open-system model as above. The equivalent age using a closed-system model is 79 ±9 days. There could be errors in estimated ^{7}Be:^{210}Pb aerosol ages due to the lack of a fixed production ratio or any fractionation that might occur between ^{7}Be and ^{210}Pb. However, in a companion work (*Landis et al. in review*) we measured ^{7}Be:^{10}Be ratios in bulk deposition for which interpretation is unambiguous (*Graham et al.* 2003). Our estimated open-system ages for >0.5 µm insoluble particulates in rainwater =260 ±45 days. Importantly, the soluble (<0.5 µm) fraction was significantly younger (120 ±30 days). This demonstrates that the two fractions are geochemically distinct and must represent different aerosol populations. These observations suggest that FRNs recirculate as fine aerosols in the terrestrial environment for an extended period following deposition. Taken together, terrestrial aerosol aging and resuspension appears to be a universal and predictable phenomenon. More work will be required to understand implications for mass budgets of FRNs and aerosols (*Saylor et al. 2019*), exposure risks due to co-pollutants (*Kinase et al. 2018*), and climate feedbacks (*Boucher et al. 2013*).

5.3. Implications of multiple aerosol populations for FRN tracer applications

Our discussion of factors influencing FRN deposition leads us to conclude that a minimum of four distinct aerosol populations contribute to FRN deposition. These include rainout and washout fractions of wet deposition, ambient PM10, and resuspended aerosol or dust. Such a diverse assemblage suggests a complex behavior in terrestrial systems. The prevailing assumptions that FRN aerosols behave congruently during deposition have relied on observations of ambient PM aerosol alone-- that ^{7}Be and ^{210}Pb share nearly identical aerosol size distributions (e.g., *Winkler et al. 1998*, *Gründel and Porstendörfer 2004*) and comparable dry depositional velocities (v_D). How we extend these assumptions

to other aerosol populations and wet processes that constitute the vast majority of FRN deposition is not clear, however. First, aerosol composition varies with altitude (*Dibb et al. 2003, Holacek et al. 2007*) and, undoubtedly, precipitation samples a different air mass than ground level sampling for ambient aerosol (*Dibb and Jaffrezo 2003*). Second, wet scavenging could discriminate aerosol populations based on their composition, size, density, electrical charge, etc. (*Seinfeld and Pandis 2016*, *Bourcier et al. 2014*, *Blanco-Allegre et al. 2018*). Discrimination through aerosol scavenging and formation of condensation nuclei may cause precipitation to be preferentially enriched in plant waxes, biogenic components, oxidized polar and aromatic compounds, and mineral dust, for example (*Simoneit and Mazurek 1989, Holacek et al. 2007*).

The influence of scavenging processes on FRNs is not well understood (*Baskaran 2011*). Some insight comes from the few available comparisons of cloudwater and rain FRN concentrations. In the definitive work, *Su and Huh* (*2006*) showed that ^{7}Be and ^{210}Pb partition to raindrops with equal efficiency (cloud:rain efficiency $\approx$1, n >50), and that both are dependent on cloudwater pH. Conversely, *Bourcier et al.* (*2014*) showed some evidence that ^{210}Pb may partition preferentially to rain, but their measurements were few (^{7}Be:^{210}Pb cloud:rain efficiency =2.4 $\pm$2.2, n=8), and contributing factors were not explored (e.g., mixing of different airmasses and aerosol population). It is nonetheless important to consider what properties could drive incongruence between the FRNs. Here, our solubility index showed higher solubility of ^{7}Be than ^{210}Pb in precipitation. It has likewise been shown that ^{7}Be in PM2.5 is almost entirely soluble in water (*Bloom and Crecelius 1983, Bondietti et al. 1988*). The solubility of ^{7}Be in PM10 is similarly high with an average of 81% removed in deionized water, but only 28% of ^{210}Pb (*Landis et al. in review*). Similarly, in filtered rainwater 80% of ^{7}Be was found in a <0.5 um fraction whereas 48% ^{210}Pb was found there (*Landis et al. in review*; *Gaffney et al. 1994*). Beyond the FRNs themselves, the MTE composition of precipitation changes significantly through the washout-rainout transition, and this might influence FRN speciation as well. For example, we found specific affinities of ^{210}Pb for SO_4 and ^{7}Be for N^P. Formation of $PbSO_4$ could contribute to lower ^{210}Pb solubility (Section 4.5).

In summary, solubility differences, divergent chemistries or resuspension of aged aerosols all could lead to a larger activity size-distribution of ^{210}Pb in rainwater, and thus to higher scavenging efficiencies (*Flossman et al. 1985*). We must therefore conclude that, when comparing bulk deposition of ^{7}Be and ^{210}Pb, differences in aerosol altitude, transport (recharge), size and chemistry all may dictate evolution of the ^{7}Be:^{210}Pb ratio. These are the primary contributors to incongruence in the ^{7}Be and ^{210}Pb pair and are the likely reasons why even stable Pb and ^{210}Pb, for example, are discriminated through the washout-rainout transition (*Talbot and Andren 1983*), interact differently with vegetation (*Shotyk et al. 2015*), and exhibit different partitioning behaviors in natural waters (*Benoit 1995*). In exploring these influences on FRN tracer applications, future work might emphasize the ^{7}Be:^{10}Be pair for additional constraints for ^{7}Be:^{210}Pb tracer applications.

6. Summary

We described a continuous, 9-year record of weekly bulk deposition of the fallout radionuclides (FRNs) ^{7}Be and ^{210}Pb, together with weak-acid soluble major/trace elements (MTEs) including S, Hg, Zn, V, K, P, Mn, Mg, Ca, Sr, Al, Fe, and combustible N and C. Simultaneous measurement of ^{7}Be, ^{210}Pb and S provides a context for interpreting their individual behaviors since all are secondary aerosols, produced in the atmosphere by gas-to-particle conversion. Fluxes of ^{7}Be, ^{210}Pb and S strongly covary as an expected consequence of their atmospheric production, their efficient removal by wet scavenging, and related seasonal, meteorological and micro-meteorological controls.

Despite their strong commonalities, by applying multiple regression techniques we found that ^{7}Be, ^{210}Pb and S each associate with unique mixtures of aerosol populations. These mixtures are controlled by their production sources (high/low altitude, cosmogenic, radiogenic, combustion, etc.); dominant depositional mechanisms (rainout, washout, dry); meteorological conditions that drive vertical and lateral atmospheric mixing (convection/stability and advection), major/trace element (MTE) chemistries of characteristic aerosols; seasonal controls on production; and particle aging (resuspension of aged aerosols and the different half-lives of ^{7}Be and ^{210}Pb). We use a ^{7}Be:^{210}Pb chronometer to show that, globally, a significant fraction of secondary aerosol deposition remains in recirculation and resuspension for an average period of around 200 days.

Through these controls ^{7}Be, ^{210}Pb and S each have unique depositional behaviors. ^{7}Be is favored by the rainout process as a consequence of its higher altitude of production and stronger synoptic atmospheric recharge between storm events, and thus best traces long-range aerosol transport. ^{7}Be is abundant in marine moisture sources, a characteristic shared by biogenic aerosols including K, P, particulate N and C. A strong correlation of ^{7}Be with N^{P} and P, independent of moisture source, suggests that biogenic aerosols may play an important role in ^{7}Be scavenging and deposition. Finally, ^{7}Be is enriched in spring/summer deposition due to stratospheric influence and is weakly influenced by solar modulation (11-year cycle).

In contrast, ^{210}Pb is favored by dry and washout deposition as a consequence of its terrestrial (low altitude) source. It is enriched in convective storms that drive vertical mixing and depleted in marine moisture sources where ^{210}Pb production is low. Both characteristics are shared with S and lithogenic elements Fe, Al, Mg. Further, ^{210}Pb shows a significant correlation with S that is independent of meteorological controls. Half of this effect is attributable to long-term declines in both S (14% y^{-1}) and ^{210}Pb (4% y^{-1}) over the past decade, possibly indicating an active role of SO_4 in scavenging of ^{210}Pb aerosols and a limitation of ^{210}Pb solubility. We attribute enhanced ^{210}Pb flux in autumn, in conjunction with elevated Mn, Hg and V, to the resuspension of biogenic dust during annual tree leaf fall. While we identified no independent correlation of ^{210}Pb deposition with these elements, aerosol or dust mass, ^{7}Be:^{210}Pb ratios were lower in bulk

dry deposition and washout versus ambient PM10 aerosol. This confirms resuspension of an aged aerosol fraction, with lower ^{7}Be:^{210}Pb ratios due to rapid radioactive decay of ^{7}Be. By indexing this fraction to particulate C we estimate that the recycled fraction of annual ^{210}Pb deposition contributes a maximum of 0.2-5%, and is likely <1%.

Finally, deposition of S is favored by dry deposition of SO_2 and rainout of SO_4, is enhanced in convective storms and depleted in marine moisture sources. Significant, independent correlations of S with ^{210}Pb, anthropogenic elements Zn, Hg and V, and biogenic elements P, K and N, demonstrate a complex mixture of sources that varies seasonally. We observed a long-term decline in S deposition which is due to well-recognized reductions in anthropogenic emissions. We speculate that this decline may impact scavenging of ^{210}Pb and other metals through formation of $PbSO_4$ and other mineral sulfates.

Variations in ^{7}Be:^{210}Pb ratios of bulk atmospheric deposition reflect the mixing of distinct aerosol populations over spatial and temporal scales. Locally, ^{7}Be:^{210}Pb ratios are controlled by the degree of atmospheric vertical mixing and the lateral mixing of different moisture source, by precipitation depth (p_D) via a washout-rainout transition, and by seasonality through intrusion of ^{7}Be-rich stratospheric air and autumnal resuspension of biogenic dust. Globally, these controls are expressed climatically through synoptic-scale weather patterns. Latitudinal and longitudinal controls on ^{7}Be and ^{210}Pb production (*Preiss et al. 1996*, *Baskaran 2011*, *Du et al. 2015*) are necessary but insufficient to drive ^{7}Be:^{210}Pb variations in global deposition. North American/European (NAE) ratios are controlled by p_D due to the proximity of these sites to the polar jet and mid-latitude storm tracks which efficiently recharge ^{7}Be aerosols between storm events through an advective process. For Southeast/East Asian (SEA) sites, FRN deposition is dominated by a dilutative effect with ^{7}Be:^{210}Pb ratios independent of p_D.

Mixtures of different ^{7}Be and ^{210}Pb aerosols are likely to differ spatially and temporally, and implications for the subsequent behaviors of the FRNs in terrestrial tracer applications should be investigated further. Nonetheless, it is an encouraging observation from global data, that site-specific mean ^{7}Be:^{210}Pb flux ratios (and by extension, related aerosol characteristics) are consistent and predictable year to year. For North American and European sites this presents a discontinuity across scales -- ^{7,10}Be:Pb ratios increase with precipitation both within single storm events and at global synoptic scales, but not with interannual variability in total precipitation. This means that there is local constancy in source terms for terrestrial tracer applications. We interpret this as a climatic limitation on synoptic recharge and, as a result, annual ^{7,10}Be fluxes and ^{7,10}Be:^{210}Pb ratios are consistent year-to-year in a stable climate. Future patterns in FRN deposition or interpretation of paleorecords may be complicated if storm tracks shift in response to a changing climate regime (e.g., *Ouimet et al. 2015*).

Acknowledgements

JDL thanks Erich Osterberg for helpful discussions on meteorology that guided and improved the manuscript. Contributions by CER were supported by National Science Foundation EAR-1545623. We declare no conflicts of interest with respect to results presented here. Data that support this paper may be found at: http://dx.doi.org/10.17632/75d9k6wysr.1

References

Aas, W., Mortier, A., Bowersox, V., Cherian, R., Faluvegi, G., Fagerli, H., et al. (2019). Global and regional trends of atmospheric sulfur. *Scientific Reports*, *9*(1), 1–11. https://doi.org/10.1038/s41598-018-37304-0

Akata, N., Kawabata, H., Hasegawa, H., Sato, T., Chikuchi, Y., Kondo, K., et al. (2008). Total deposition velocities and scavenging ratios of 7Be and 210Pb at Rokkasho, Japan. *Journal of Radioanalytical and Nuclear Chemistry*, *277*(2), 347–355. https://doi.org/10.1007/s10967-007-7095-1

Aldahan, A., Hedfors, J., Possnert, G., Kulan, A., Berggren, A. M., & Söderström, C. (2008). Atmospheric impact on beryllium isotopes as solar activity proxy. *Geophysical Research Letters*, *35*(21), 1–5. https://doi.org/10.1029/2008GL035189

Alonso-Hernández, C. M., Morera-Gómez, Y., Cartas-Águila, H., & Guillén-Arruebarrena, A. (2014). Atmospheric deposition patterns of ^{210}Pb and ^{7}Be in Cienfuegos, Cuba. *Journal of Environmental Radioactivity*, *138*, 149–155. https://doi.org/10.1016/j.jenvrad.2014.08.023

Andronache, C. (2003). Estimated variability of below-cloud aerosol removal by rainfall for observed aerosol size distributions. *Atmospheric Chemistry and Physics*, *3*(1), 131–143. https://doi.org/10.5194/acp-3-131-2003

Anspaugh, L. R., Simon, S. L., Gordeev, K. I., Likhtarev, I. A., Maxwell, R. M., & Shinkarev, S. M. (2002). Movement of radionuclides in terrestrial ecosystems by physical processes. *Health Physics*, *82*(5), 669–679. https://doi.org/10.1097/00004032-200205000-00013

Appleby, P. G., & Oldfield, F. (1978). The calculation of lead-210 dates assuming a constant rate of supply of unsupported 210Pb to the sediment. *Catena*, *5*(1), 1–8. https://doi.org/10.1016/S0341-8162(78)80002-2

Appleby, P. G., Koulikov, A. O., Camarero, L., & Ventura, M. (2002). The input and transmission of fallout radionuclides through Redo, a high mountain lake in the Spanish Pyrenees. *Water, Air, & Soil Pollution: Focus*. https://doi.org/10.1023/A

Appleby, P. G., Semertzidou, P., Piliposian, G. T., Chiverrell, R. C., Schillereff, D. N., & Warburton, J. (2003). The transport and mass balance of fallout radionuclides in Brotherswater, Cumbria (UK). *Journal of Paleolimnology*, *62*(4), 389–407. https://doi.org/10.1007/s10933-019-00095-z

Arnold, J. R., & Al-Salih, H. a. (1955). Beryllium-7 produced by cosmic eays. *Science*, *121*(3144), 451–3. https://doi.org/10.1126/science.121.3144.451

Barg, E., Lal, D., Pavich, M. J., Caffee, M. W., & Southon, J. R. (1997). Beryllium geochemistry in soils: Evaluation of $^{10}Be/^{9}Be$ ratios in authigenic minerals as a basis for age models. *Chemical Geology*, *140*(3–4), 237–258. https://doi.org/10.1016/S0009-2541(97)00051-X

Baskaran, M. (1995). A search for the seasonal variability on the depositional fluxes of ^{7}Be and ^{210}Pb. *Journal of Geophysical Research*, *100*(D2), 2833–2840. https://doi.org/10.1029/94JD02824

Baskaran, M. (2011). Po-210 and Pb-210 as atmospheric tracers and global atmospheric Pb-210 fallout: A Review. *Journal of Environmental Radioactivity*, *102*(5), 500–513. https://doi.org/10.1016/j.jenvrad.2010.10.007

Baskaran, M., Coleman, C. H., & Santschi, P. H. (1993). Atmospheric depositional fluxes of ^{7}Be and ^{210}Pb at Galveston and College Station, Texas. *Journal of Geophysical Research*, *98*(D11). https://doi.org/10.1029/93jd02182

Baskaran, M., & Swarzenski, P. W. (2007). Seasonal variations on the residence times and partitioning of short-lived radionuclides (234Th, 7Be and 210Pb) and depositional fluxes of ^{7}Be and ^{210}Pb in Tampa Bay, Florida. *Marine Chemistry*, *104*(1–2), 27–42. https://doi.org/10.1016/j.marchem.2006.06.012

Batonneau, Y., Bremard, C., Gengembre, L., Laureyns, J., Le Maguer, A., Le Maguer, D., et al. (2004). Speciation of PM10 sources of airborne nonferrous metals within the 3-km zone of lead/zinc smelters. *Environmental Science and Technology*, *38*(20), 5281–5289. https://doi.org/10.1021/es0497173

Baumgardner, R. E., Lavery, T. F., Rogers, C. M., & Isil, S. S. (2002). Estimates of the atmospheric deposition of sulfur and nitrogen species: Clean Air Status and Trends Network, 1990-2000. *Environmental Science and Technology*, *36*(12), 2614–2629. https://doi.org/10.1021/es011146g

Belis, C. A., Karagulian, F., Larsen, B. R., & Hopke, P. K. (2013). Critical review and meta-analysis of ambient particulate matter source apportionment using receptor models in Europe. *Atmospheric Environment*, *69*, 94–108. https://doi.org/10.1016/j.atmosenv.2012.11.009

Benitez-nelson, C. R., & Buesseler, K. O. (1999). Phosphorous-32, phosphorous-37, beryllium-7, and lead-210: Atmospheric fluxes and utility in tracing stratosphere/troposphere exchange. *Journal of Geophysical Research*, *104*(D9), 11745–11754.

Benoit, G. (1995). Evidence of the particle concentration effect for lead and other metals in fresh waters based on ultraclean technique analyses. *Geochimica et Cosmochimica Acta*, *59*(13), 2677–2687. https://doi.org/10.1016/0016-7037(95)00164-U

Biggins, P. D. E., & Harrison, R. M. (1979). Characterization and classification

of atmospheric sulfates. *Journal of the Air Pollution Control Association*, *29*(8), 838–840. https://doi.org/10.1080/00022470.1979.10470871

Blake, W. H., Walling, D. E., & He, Q. (1999). Fallout beryllium-7 as a tracer in soil erosion investigations. *Applied Radiation and Isotopes*, *51*(5), 599–605.

Blanco-Alegre, C., Castro, A., Calvo, A. I., Oduber, F., Alonso-Blanco, E., Fernández-González, D., et al. (2018). Below-cloud scavenging of fine and coarse aerosol particles by rain: The role of raindrop size. *Quarterly Journal of the Royal Meteorological Society*, *144*(717), 2715–2726. https://doi.org/10.1002/qj.3399

Bloom, N., & Crecelius, E. A. (1983). Solubility behavior of atmospheric ^{7}Be in the marine environment. *Marine Chemistry*, *12*, 323–331.

Bondietti, E. A., Brantley, J. N., & Rangarajan, C. (1988). Size distributions and growth of natural and Chernobyl-derived submicron aerosols in Tennessee. *Journal of Environmental Radioactivity*, *6*(2), 99–120. https://doi.org/10.1016/0265-931X(88)90054-9

Bonniwell, E. C., Matisoff, G., & Whiting, P. J. (1999). Determining the times and distances of particle transit in a mountain stream using fallout radionuclides. *Geomorphology*, *27*(1–2), 75–92. https://doi.org/10.1016/S0169-555X(98)00091-9

Boschi, V., & Willenbring, J. K. (2016). The effect of pH, organic ligand chemistry and mineralogy on the sorption of beryllium over time. *Environmental Chemistry*, *13*(4), 711–722. https://doi.org/10.1071/EN15107

Boucher, O., Randall, D., Artaxo, P., Bretherton, C., Feingold, G., Forster, P., et al. (2013). Clouds and Aerosols. In T. F. Stocker, D. Qin, G.-K. Plattner, M. Tignor, S. K. Allen, J. Boschung, et al. (Eds.), *Climate Change 2013: The Physical Science Basis. Contribution of Working Group I to the FIfth Assessment Report of the Intergovernmental Panel on Climate Change*. Cambridge: Cambridge University Press.

Bourcier, L., Masson, O., Laj, P., Paulat, P., Pichon, J.-M. et al. (2014). ^{7}Be, ^{210}Pb and ^{137}Cs concentrations in cloud water. *J. Environmental Radioactivity*, *128*, 15-19. http://dx.doi.org/10.1016/j.jenvrad.2013.10.020

Brown, L., Stensland, G. J., Klein, J., & Middleton, R. (1989). Atmospheric deposition of ^{7}Be and ^{10}Be. *Geochimica et Cosmochimica Acta*, *53*, 135–142.

Burgos, W. D., Castillo-Meza, L., Tasker, T. L., Geeza, T. J., Drohan, P. J., Liu, X., et al. (2017). Watershed-Scale Impacts from Surface Water Disposal of Oil and Gas Wastewater in Western Pennsylvania. *Environmental Science and Technology*, *51*(15). https://doi.org/10.1021/acs.est.7b01696

Caillet, S., Arpagaus, P., Monna, F., & Dominik, J. (2001). Factors controlling ^{7}Be and ^{210}Pb atmospheric deposition as revealed by sampling individual

rain events in the region of Geneva, Switzerland. *Journal of Environmental Radioactivity*, *53*(2), 241–256. https://doi.org/10.1016/S0265-931X(00)00130-2

Chen, J., Luo, S., & Huang, Y. (2016). Scavenging and fractionation of particle-reactive radioisotopes ^{7}Be, ^{210}Pb and ^{210}Po in the atmosphere. *Geochimica et Cosmochimica Acta*, *188*, 208–223. https://doi.org/10.1016/j.gca.2016.05.039

Chen, L., & Duce, R. A. (1983). The sources of sulfate, vanadium and mineral matter in aerosol particles over Bermunda. *Atmospheric Environment (1967)*, *17*(10), 2055–2064. https://doi.org/10.1016/0004-6981(83)90362-1

Cho, H. M., Hong, Y. L., & Kim, G. (2011). Atmospheric depositional fluxes of cosmogenic ^{35}S and ^{7}Be: Implications for the turnover rate of sulfur through the biosphere. *Atmospheric Environment*, *45*(25), 4230–4234. https://doi.org/10.1016/j.atmosenv.2011.05.002

Chuang, C. Y., Santschi, P. H., Wen, L. S., Guo, L., Xu, C., et al. (2015) Binding of Th, Pa, Pb, Po and Be radionuclides to marine colloidal macromolecular organic matter. *Mar. Chem. 173*, 320-329.

Clifton, R. J., Watson, P. G., Davey, J. T., & Frickers, P. E. (1995). A study of processes affecting the uptake of contaminants by intertidal sediments, using the radioactive tracers: ^{7}Be, ^{137}Cs and unsupported ^{210}Pb. *Estuarine, Coastal and Shelf Science*, *41*(4), 459–474. https://doi.org/10.1016/0272-7714(95)90004-7

Creamean, J. M., Lee, C., Hill, T. C., Ault, A. P., DeMott, P. J., White, A. B., et al. (2014). Chemical properties of insoluble precipitation residue particles. *Journal of Aerosol Science*, *76*, 13–27. https://doi.org/10.1016/j.jaerosci.2014.05.005

Cutshall, N. H., Larsen, I. L., & Olsen, C. R. (1983). Direct analysis of ^{210}Pb in sediment samples: self-absorption corrections. *Nuclear Instruments and Methods in Physics Research Section A*, *206*(1–2), 309–312.

Delaygue, G., Bekki, S., & Bard, E. (2015). Modelling the stratospheric budget of beryllium isotopes. *Tellus, Series B: Chemical and Physical Meteorology*, *67*(1). https://doi.org/10.3402/tellusb.v67.28582

Dibb, J. E. (1989). Atmospheric deposition of beryllium-7 in the Chesapeake Bay region. *Journal of Geophysical Research*, *94*(D2), 2261–2265. https://doi.org/10.1029/JD094iD02p02261

Dibb, J. E., Talbot, R. W., & Gregory, G. L. (1992). Beryllium-7 and lead-210 in the western hemisphere Arctic atmosphere: observations from three recent aircraft-based sampling programs. *Journal of Geophysical Research*, *97*(D15). https://doi.org/10.1029/91jd01807

Dibb, J. E., & Jaffrezo, J.-L. (1993). Beryllium-7 and lead-210 in aerosol and snow in the DYE 3 gas, aerosol and snow sampling program. *Atmos. Environ.*, *27*(17), 2751–2760.

Dibb, J. E., Talbot, R. W., Scheuer, E. M., Seid, G., Avery, M. A., & Singh, H. B. (2003). Aerosol chemical composition in Asian continental outflow during the TRACE-P campaign: Comparison with PEM-West B. *Journal of Geophysical Research D: Atmospheres*, *108*(21), 1–13. https://doi.org/10.1029/2002jd003111

Dixon, J. L., Chadwick, O. A., & Pavich, M. J. (2018). Climatically controlled delivery and retention of meteoric ^{10}Be in soils. *Geology*, *46*(10), 899–902. https://doi.org/10.1130/G45176.1

Długosz-Lisiecka, M., & Bem, H. (2012). Determination of the mean aerosol residence times in the atmosphere and additional ^{21}0Po input on the base of simultaneous determination of ^{7}Be, ^{22}Na, ^{210}Pb, ^{210}Bi and ^{210}Po in urban air. *Journal of Radioanalytical and Nuclear Chemistry*, *293*(1), 135–140. https://doi.org/10.1007/s10967-012-1690-5

Dominik, J., Burrus, D., & Vernet, J. (1987). Transport of the environmental radionuclides in an alpine watershed. *Earth and Planetary Science Letters*, *84*, 165–180.

Driscoll, C. T., Mason, R. P., Chan, H. M., Jacob, D. J., & Pirrone, N. (2013). Mercury as a global pollutant: Sources, pathways, and effects. *Environmental Science and Technology*, *47*(10), 4967–4983. https://doi.org/10.1021/es305071v

Du, J., Baskaran, M., Bi, Q., Huang, D., & Jiang, Y. (2015). Temporal variations of atmospheric depositional fluxes of ^{7}Be and ^{210}Pb over 8 years (2006-2013) at Shanghai, China, and synthesis of global fallout data. *J Geophys Res*, *120*, 4323–4339. https://doi.org/10.1038/175238c0

Dueñas, C., Gordo, E., Liger, E., Cabello, M., Cañete, S., Pérez, M., & Torre-Luque, P. de la. (2017). ^{7}Be, ^{210}Pb and ^{40}K depositions over 11 years in Málaga. *Journal of Environmental Radioactivity*, *178–179*, 325–334. https://doi.org/10.1016/j.jenvrad.2017.09.010

Dugan, H. A., Bartlett, S. L., Burke, S. M., Doubek, J. P., Krivak-Tetley, F. E., Skaff, N. K., et al. (2017). Salting our freshwater lakes. *Proceedings of the National Academy of Sciences of the United States of America*, *114*(17), 4453–4458. https://doi.org/10.1073/pnas.1620211114

Eckley, C. S., Tate, M. T., Lin, C. J., Gustin, M., Dent, S., Eagles-Smith, C., et al. (2016). Surface-air mercury fluxes across Western North America: A synthesis of spatial trends and controlling variables. *Science of the Total Environment*, *568*, 651–665. https://doi.org/10.1016/j.scitotenv.2016.02.121

Evrard, O., Némery, J., Gratiot, N., Duvert, C., Ayrault, S., Lefèvre, I., et al. (2010). Sediment dynamics during the rainy season in tropical highland catchments of central Mexico using fallout radionuclides. *Geomorphology*, *124*(1–2), 42–54. https://doi.org/10.1016/j.geomorph.2010.08.007

Fang, T., Guo, H., Zeng, L., Verma, V., Nenes, A., & Weber, R. J. (2017). Highly acidic ambient particles, soluble Metals, and oxidative potential: A link

between sulfate and aerosol toxicity. *Environmental Science and Technology*, *51*(5), 2611–2620. https://doi.org/10.1021/acs.est.6b06151

Farmer, J. G., Eades, L. J., Graham, M. C., Cloy, J. M., & Bacon, J. R. (2010). A comparison of the isotopic composition of lead in rainwater, surface vegetation and tree bark at the long-term monitoring site, Glensaugh, Scotland, in 2007. *Science of the Total Environment*, *408*(17), 3704–3710. https://doi.org/10.1016/j.scitotenv.2010.03.050

Feely H. W., & Seitz H. (1970). Use of lead-210 as a tracer of transport processes in the stratosphere. *J Geophys Res*, *75*(15), 2885–2894. https://doi.org/10.1029/jc075i015p02885

Feely, H. W., Larsen, R. J., & Sanderson, C. G. (1989). Factors that cause seasonal variations in Beryllium-7 concentrations in surface air. *Journal of Environmental Radioactivity*, *9*(3), 223–249. https://doi.org/10.1016/0265-931X(89)90046-5

Field, C. V., Schmidt, G. A., Koch, D., & Salyk, C. (2006). Modeling production and climate-related impacts on 10Be concentration in ice cores. *Journal of Geophysical Research Atmospheres*, *111*.

Fitzgerald, S. A., Klump, J. V, Swarzenski, P. W., Mackenzie, R. A., & Richards, K. D. (2001). Beryllium-7 as a tracer of short-term sediment deposition and resuspension in the Fox River, Wisconsin. *Environmental Science & Technology*, *35*(2), 300–5.

Flossman, A. I., Hall, W. D., & Pruppacher, H. R. (1985). A theoretical study of the wet removal of atmospheric pollutants. Part I: the redistribution of aerosol particles captured through nucleation and impaction scavenging by growing cloud drops. *Journal of the Atmospheric Sciences*, *42*(6), 583–606.

Fuzzi, S., Baltensperger, U., Carslaw, K., Decesari, S., Denier Van Der Gon, H., Facchini, M. C., et al. (2015). Particulate matter, air quality and climate: Lessons learned and future needs. *Atmospheric Chemistry and Physics*, *15*(14), 8217–8299. https://doi.org/10.5194/acp-15-8217-2015

Gaffney, J. S., Orlandini, K. A., & Marley, N. A. (1994). Measurements of ^{7}Be and ^{210}Pb in rain, snow and hail. *Journal of the American Meteorological Society*, *33*, 869–873.

Garland, J. A., & Pomeroy, I. R. (1994). Resuspension of fall-out material following the Chernobyl accident. *Journal of Aerosol Science*, *25*(5), 793–806.

Gartner, J. D., Renshaw, C. E., Dade, W. B., & Magilligan, F. J. (2012). Time and depth scales of fine sediment delivery into gravel stream beds: Constraints from fallout radionuclides on fine sediment residence time and delivery. *Geomorphology*, *151–152*, 39–49. https://doi.org/10.1016/j.geomorph.2012.01.008

Gonzalez, R. O., Strekopytov, S., Amato, F., Querol, X., Reche, C., & Weiss, D. (2016). New Insights from zinc and copper isotopic composi-

tions into the sources of atmospheric particulate matter from two major European cities. *Environmental Science and Technology*, *50*(18), 9816–9824. https://doi.org/10.1021/acs.est.6b00863

Gourdin, E., Evrard, O., Huon, S., Reyss, J. L., Ribolzi, O., Bariac, T., et al. (2014). Spatial and temporal variability of ^{7}Be and ^{210}Pb wet deposition during four successive monsoon storms in a catchment of northern Laos. *Journal of Environmental Radioactivity*, *136*, 195–205. https://doi.org/10.1016/j.jenvrad.2014.06.008

Graham, I., Ditchburn, R., & Barry, B. (2003). Atmospheric deposition of ^{7}Be and ^{10}Be in New Zealand rain (1996-98). *Geochemica et Cosmochimica Acta*, *67*(3), 361–373.

Graly, J. A., Reusser, L. J., & Bierman, P. R. (2011). Short and long-term delivery rates of meteoric ^{10}Be to terrestrial soils. *Earth and Planetary Science Letters*, *302*(3–4), 329–336. https://doi.org/10.1016/j.epsl.2010.12.020

Gründel, M., & Porstendörfer, J. (2004). Differences between the activity size distributions of the different natural radionuclide aerosols in outdoor air. *Atmospheric Environment*, *38*(22), 3723–3728. https://doi.org/10.1016/j.atmosenv.2004.01.043

Guo, H., Nenes, A., & Weber, R. J. (2018). The underappreciated role of nonvolatile cations in aerosol ammonium-sulfate molar ratios. *Atmospheric Chemistry and Physics*, *18*(23), 17307–17323. https://doi.org/10.5194/acp-18-17307-2018

He, Q., & Walling, D. E. (1996). Use of fallout Pb-210 measurements to investigate longer-term rates and patterns of overbank sediment deposition on the floodplains of lowland rivers. *Earth Surface Processes and Landforms*, *21*(2), 141–154

Hirose, K., Honda, T., Yagishita, S., Igarashi, Y., & Aoyama, M. (2004). Deposition behaviors of ^{210}Pb, ^{7}Be and thorium isotopes observed in Tsukuba and Nagasaki, Japan. *Atmospheric Environment*, *38*(38), 6601–6608. https://doi.org/10.1016/j.atmosenv.2004.08.012

Holecek, J. C., Spencer, M. T., & Prather, K. A. (2007). Analysis of rainwater samples: Comparison of single particle residues with ambient particle chemistry from the northeast Pacific and Indian oceans. *Journal of Geophysical Research Atmospheres*, *112*(22). https://doi.org/10.1029/2006JD008269

Hu, J., Sha, Z., Wang, J., Du, J., & Ma, Y. (2020). Atmospheric deposition of ^{7}Be, ^{210}Pb in Xining, a typical city on the Qinghai-Tibet Plateau, China. *Journal of Radioanalytical and Nuclear Chemistry*, *324*(3), 1141–1150. https://doi.org/10.1007/s10967-020-07127-3

Huang, H., Winter, J. M., & Osterberg, E. C. (2018). Mechanisms of abrupt extreme precipitation change over the northeastern United States. *Journal of Geophysical Research: Atmospheres*, *123*(14), 7179–7192. https://doi.org/10.1029/2017JD028136

Huh, C. A., Su, C. C., & Shiau, L. J. (2006). Factors controlling temporal and spatial variations of atmospheric deposition of ^{7}Be and ^{210}Pb in northern Taiwan. *Journal of Geophysical Research Atmospheres*, *111*(16), 1–7. https://doi.org/10.1029/2006JD007180

Ishikawa, Y., Murakami, H., Sekine, T., & Yoshihara, K. (1995). Precipitation scavenging studies of radionuclides in air using cosmogenic ^{7}Be. *Journal of Environmental Radioactivity*, *26*(1), 19–36. https://doi.org/10.1016/0265-931X(95)91630-M

Jaenicke, R. (1980). Natural aerosols. *Annals of The New York Academy of Sciences*, *338*, 317–329.

Jia, C., Liu, G., Yang, W., Zhang, L. and Huang, Y. (2003) Atmospheric depositional fluxes of ^{7}Be and ^{210}Pb at Xiamen, *J. Xiamen Univ.*, 42, 353-357. (Chinese language)

Jiskra, M., Sonke, J. E., Obrist, D., Bieser, J., Ebinghaus, R., Myhre, C. L., et al. (2018). A vegetation control on seasonal variations in global atmospheric mercury concentrations. *Nature Geoscience*, *11*(4), 244–250. https://doi.org/10.1038/s41561-018-0078-8

Joshi, L. U. and Mahadeavan, T. N. (1968). Seasonal variation of lead-210 in ground level air in India. *Health Physics*, *15*, 67–71.

Jungers, M. C., Bierman, P. R., Matmon, A., Nichols, K., Larsen, J., & Finkel, R. (2009). Tracing hillslope sediment production and transport with in-situ and meteoric^{10}Be. *Journal of Geophysical Research: Earth Surface*, *114*(4), 1–16. https://doi.org/10.1029/2008JF001086

Karwan, D. L., Pizzuto, J. E., Aalto, R., Marquard, J., Harpold, A., Skalak, K., et al. (2018). Direct channel precipitation and storm characteristics influence short-term fallout radionuclide assessment of sediment source. *Water Resources Research*, *54*(7), 4579–4594. https://doi.org/10.1029/2017WR021684

Kaste, J. M., & Baskaran, M. (2011). Handbook of environmental isotope geochemistry. *Handbook of Environmental Isotope Geochemistry*, *1–2*(January 2011), 1–951. https://doi.org/10.1007/978-3-642-10637-8

Kaste, J. M., Friedland, A. J., & Stürup, S. (2003). Using stable and radioactive isotopes to trace atmospherically deposited Pb in montane forest soils. *Environmental Science & Technology*, *37*(16), 3560–7.

Kaste, J. M., Bostick, B. C., Heimsath, A. M., Steinnes, E., & Friedland, A. J. (2011). Using atmospheric fallout to date organic horizon layers and quantify metal dynamics during decomposition. *Geochimica et Cosmochimica Acta*, *75*(6), 1642–1661. https://doi.org/10.1016/j.gca.2011.01.011

Kim, G., Alleman, Y., & Church, M. (1999). Atmospheric depositional fluxes of trace elements, ^{210}Pb and ^{7}Be to the Sargasso Sea. *Global Biogeochemical Cycles*, *13*(4), 1183–1192.

Kim, G., Hussain, N., Scudlark, J. R., & Church, T. M. (2000). Factors influencing the atmospheric depositional fluxes of stable Pb, ^{210}Pb, and ^{7}Be into Chesapeake Bay. *Journal of Atmospheric Chemistry*, *36*(1), 65–79. https://doi.org/10.1023/A:1006383030362

Kim, S. H., Hong, G. H., Baskaran, M., Park, K. M., Chung, C. S. & Kim, K. H. (1998) Wet removal of atmospheric ^{7}Be and ^{210}Pb at the Korean Yellow Sea Coast, *Yellow Sea*, *4*, 58-68.

Kinase, T., Kita, K., Igarashi, Y., Adachi, K., Ninomiya, K., Shinohara, A., et al. (2018). The seasonal variations of atmospheric 134,137Cs activity and possible host particles for their resuspension in the contaminated areas of Tsushima and Yamakiya, Fukushima, Japan. *Progress in Earth and Planetary Science*, *5*(1). https://doi.org/10.1186/s40645-018-0171-z

Klaminder, J., Bindler, R., Emteryd, O., Appleby, P., & Grip, H. (2006). Estimating the mean residence time of lead in the organic horizon of boreal forest soils using 210-lead, stable lead and a soil chronosequence. *Biogeochemistry*, *78*(1), 31–49. https://doi.org/10.1007/s10533-005-2230-y

Koch, D. M., Jacob, D. J., & Graustein, W. C. (1996). Vertical transport of tropospheric aerosols as indicated by ^{7}Be and ^{210}Pb in a chemical tracer model. *Journal of Geophysical Research Atmospheres*, *101*(13), 18651–18666. https://doi.org/10.1029/96jd01176

Kownacka, L. (2002). Vertical distributions of beryllium-7 and lead-210 in the tropospheric and lower stratospheric air. *Nukleonika*, *47*(2), 79–82.

Laguionie, P., Roupsard, P., Maro, D., Solier, L., Rozet, M., Hébert, D., & Connan, O. (2014). Simultaneous quantification of the contributions of dry, washout and rainout deposition to the total deposition of particle-bound ^{7}Be and ^{210}Pb on an urban catchment area on a monthly scale. *Journal of Aerosol Science*, *77*, 67–84. https://doi.org/10.1016/j.jaerosci.2014.07.008

Lal, D., Nijampurkar, V. N., Rajagopalan, G., and Somayajulu, B. L. K.: Annual fallout of ^{32}Si, ^{210}Pb, ^{22}Na, ^{35}S and ^{7}Be in rains in India, *Proc. Indian Acad. Sci.*, *88*, 29-40, 1979.

Landis, J. D., Renshaw, C. E., & Kaste, J. M. (2012a). Measurement of 7Be in soils and sediments by gamma spectroscopy. *Chemical Geology*, *291*, 175–185. https://doi.org/10.1016/j.chemgeo.2011.10.007

Landis, J. D., Renshaw, C. E., & Kaste, J. M. (2014). Quantitative retention of atmospherically deposited elements by native vegetation is traced by the fallout radionuclides ^{7}Be and ^{210}Pb. *Environmental Science and Technology*, *48*(20), 12022–12030. https://doi.org/10.1021/es503351u

Landis, J. D., Renshaw, C. E., & Kaste, J. M. (*in review*). Sorption behavior and aerosol-particulate transitions of ^{7}Be, ^{10}Be and ^{210}Pb: a basis for fallout radionuclide chronometry. *Environmental Science and Technology*

Landis, J. D., Hamm, N. T., Renshaw, C. E., Dade, W. B., Magilligan, F. J., & Gartner, J. D. (2012b). Surficial redistribution of fallout ^{131}iodine in a small temperate catchment. *Proceedings of the National Academy of Sciences of the United States of America*, *109*(11), 4064–9. https://doi.org/10.1073/pnas.1118665109

Landis, J. D., Renshaw, C. E., & Kaste, J. M. (2016). Beryllium-7 and lead-210 chronometry of modern soil processes: The Linked Radionuclide aCcumulation model, LRC. *Geochimica et Cosmochimica Acta*, *180*, 109–125. https://doi.org/10.1016/j.gca.2016.02.013

Landre, A. L., Watmough, S. A., & Dillon, P. J. (2010). Metal pools, fluxes, and budgets in an acidified forested catchment on the precambrian shield, central Ontario, Canada. *Water, Air, and Soil Pollution*, *209*(1–4), 209–228. https://doi.org/10.1007/s11270-009-0193-7

Lawrence, C. R., & Neff, J. C. (2009). The contemporary physical and chemical flux of aeolian dust: A synthesis of direct measurements of dust deposition. *Chemical Geology*, *267*(1–2), 46–63. https://doi.org/10.1016/j.chemgeo.2009.02.005

Leppänen, A. P. (2019). Deposition of naturally occurring ^{7}Be and ^{210}Pb in Northern Finland. *Journal of Environmental Radioactivity*, *208–209*. https://doi.org/10.1016/j.jenvrad.2019.105995

Lin, P., Xu, C., Xing, W., Sun, L., Kaplan, D. I., Fujitake, N., et al. (2018). Radionuclide uptake by colloidal and particulate humic acids obtained from 14 soils collected worldwide. *Scientific Reports*, *8*(1), 1–11. https://doi.org/10.1038/s41598-018-23270-0

Liu, H., Considine, D. B., Horowitz, L. W., Crawford, J. H., Rodriguez, J. M., Strahan, S. E., et al. (2016). Using beryllium-7 to assess cross-tropopause transport in global models. *Atmospheric Chemistry and Physics*, *16*(7), 4641–4659. https://doi.org/10.5194/acp-16-4641-2016

Lozano, R. L., San Miguel, E. G., Bolívar, J. P., & Baskaran, M. (2011). Depositional fluxes and concentrations of 7Be and 210Pb in bulk precipitation and aerosols at the interface of Atlantic and Mediterranean coasts in Spain. *Journal of Geophysical Research Atmospheres*, *116*(18), 1–14. https://doi.org/10.1029/2011JD015675

Mabit, L., Benmansour, M., Abril, J. M., Walling, D. E., Meusburger, K., Iurian, a. R., et al. (2013). Fallout ^{210}Pb as a soil and sediment tracer in catchment sediment budget investigations: A review. *Earth-Science Reviews*, *138*, 335–351. https://doi.org/10.1016/j.earscirev.2014.06.007

Mahowald, N. M., Scanza, R., Brahney, J., Goodale, C. L., Hess, P. G., Moore, J. K., & Neff, J. (2017). Aerosol Deposition Impacts on Land and Ocean Carbon Cycles. *Current Climate Change Reports*, *3*(1), 16–31. https://doi.org/10.1007/s40641-017-0056-z

Marley, N. A., Gaffney, J. S., Drayton, P. J., Cunningham, M. M., Orlandini, K. A., & Paode, R. (2000). Measurement of ^{210}Pb, ^{210}Po, and ^{210}Bi in size-fractionated atmospheric aerosols: An estimate of fine-aerosol residence times. *Aerosol Science and Technology*, *32*(6), 569–583. https://doi.org/10.1080/027868200303489

Masarik, J., & Beer, J. (1999). Simulation of particle fluxes and cosmogenic nuclide production in the Earth's atmosphere. *Journal of Geophysical Research Atmospheres*, *104*(D10), 12099–12111. https://doi.org/10.1029/1998JD200091

Matisoff, G., Wilson, C. G., & Whiting, P. J. (2005). The ^{7}Be/^{210}Pb$_{xs}$ ratio as an indicator of suspended sediment age or fraction new sediment in suspension. *Earth Surface Processes and Landforms*, *30*(9), 1191–1201. https://doi.org/10.1002/esp.1270

McNeary, D., & Baskaran, M. (2003). Depositional characteristics of ^{7}Be and ^{210}Pb in southeastern Michigan. *Journal of Geophysical Research D: Atmospheres*, *108*(7). https://doi.org/10.1029/2002jd003021

Mohan, M. P., D'Souza, R. S., Nayak, S. R., Kamath, S. S., Shetty, T., Kumara, K. S., et al. (2019). Influence of rainfall on atmospheric deposition fluxes of ^{7}Be and ^{210}Pb in Mangaluru (Mangalore) at the Southwest Coast of India. *Atmospheric Environment*, *202*, 281–295. https://doi.org/10.1016/j.atmosenv.2019.01.034

Momoshima, N., Nishio, S., Kusano, Y., Fukuda, A., & Ishimoto, A. (2006). Seasonal variations of atmospheric ^{210}Pb and ^{7}Be concentrations at Kumamoto, Japan and their removal from the atmosphere as wet and dry depositions. *Journal of Radioanalytical and Nuclear Chemistry*, *268*(2), 297–304. https://doi.org/10.1556/jrnc.268.2006.2.17

Monaghan, M. C. (1989). Lead-210 is surface area and soils from California: Implications for the behavior of trace constituents in the planetary boundary layer, *Journal of Geophysical Research 94(D5)*, 6449–6456.

National Oceanic and Atmospheric Administration (NOAA) Climate Database Modernization Program (CDMP), National Climatic Data Center, Asheville, NC. https://www.wpc.ncep.noaa.gov/dailywxmap/index.html.

Nopmongcol, U., Beardsley, R., Kumar, N., Knipping, E., & Yarwood, G. (2019). Changes in United States deposition of nitrogen and sulfur compounds over five decades from 1970 to 2020. *Atmospheric Environment*, *209*(April 2019), 144–151. https://doi.org/10.1016/j.atmosenv.2019.04.018

Olsen, C. R. (1985). Atmospheric fluxes and marsh-soil inventories of ^{7}Be and ^{210}Pb. *Journal of Geophysical Research*, *90*(D6), 10487–10495. https://doi.org/10.1029/JD090iD06p10487

Ostro, B., Feng, W. Y., Broadwin, R., Green, S., & Lipsett, M. (2007). The effects of components of fine particulate air pollution on mortality in Califor-

nia: Results from CALFINE. *Environmental Health Perspectives*, *115*(1), 13–19. https://doi.org/10.1289/ehp.9281

Ouimet, W., Dethier, D., Bierman, P., Wyshnytzky, C., Shea, N., & Rood, D. H. (2015). Spatial and temporal variations in meteoric 10Be inventories and long-term deposition rates, Colorado Front Range. *Quaternary Science Reviews*, *109*, 1–12. https://doi.org/10.1016/j.quascirev.2014.11.003

Papastefanou, C., & Ioannidou, A. (2004). Beryllium-7 and solar activity. *Applied Radiation and Isotopes*, *61*(6), 1493–1495. https://doi.org/10.1016/j.apradiso.2004.03.119

Peirson, D. H., Cambray, R. S., & Spicer, G. S. (1966). Lead-210 and polonium-210 in the atmosphere. *Tellus*, *18*(2–3), 427–433. https://doi.org/10.3402/tellusa.v18i2-3.9381

Peng, A., Liu, G., Jiang, Z., Liu, G., & Liu, M. (2019). Wet depositional fluxes of ^{7}Be and ^{210}Pb and their influencing factors at two characteristic cities of China. *Applied Radiation and Isotopes*, *147*(January), 21–30. https://doi.org/10.1016/j.apradiso.2019.01.016

Pham, M. K., Povinec, P. P., Nies, H., & Betti, M. (2013). Dry and wet deposition of ^{7}Be, ^{210}Pb and ^{137}Cs in Monaco air during 1998-2010: Seasonal variations of deposition fluxes. *Journal of Environmental Radioactivity*, *120*, 45–57. https://doi.org/10.1016/j.jenvrad.2012.12.007

Poet, S. E., Moore, H. E., & Martell, E. A. (1972). Lead 210, bismuth 210, and polonium 210 in the atmosphere: Accurate ratio measurement and application to aerosol residence time determination. *Journal of Geophysical Research*, *77*(33), 6515–6527. https://doi.org/10.1029/jc077i033p06515

Prather, K. A., Hatch, C. D., & Grassian, V. H. (2008). Analysis of Atmospheric Aerosols. *Annual Review of Analytical Chemistry*, *1*(1), 485–514. https://doi.org/10.1146/annurev.anchem.1.031207.113030

Preiss, N., Melieres, M.-A., & Pourchet, M. (1996). A compilation of data on lead-210 concentration in surface air and fluxes at the air-surface and water-sediment interfaces. *Journal of Geophysical Research*, *101*(D22), 28847–28862. https://doi.org/10.1029/96JD01836/full

Pye, H. O., Nenes, A., Alexander, B., Ault, A., Barth, M., Clegg, S., et al. (2019). The acidity of atmospheric particles and clouds. *Atmospheric Chemistry and Physics Discussions*, (October), 1–143. https://doi.org/10.5194/acp-2019-889

Rea, A. W., Lindberg, S. E., Scherbatskoy, T., & Keeler, G. J. (2002). Mercury accumulation in foliage over time in two northern mixed-hardwood forests. *Water, Air, and Soil Pollution*, *133*(1–4), 49–67. https://doi.org/10.1023/A:1012919731598

Rea, A. W., Lindberg, S. E., & Keeler, G. J. (2001). Dry deposition and foliar leaching of mercury and selected trace elements in deciduous forest throughfall.

Atmospheric Environment, *35*(20), 3453–3462. https://doi.org/10.1016/S1352-2310(01)00133-9

Reddington, C. L., McMeeking, G., Mann, G. W., Coe, H., Frontoso, M. G., Liu, D., et al. (2013). The mass and number size distributions of black carbon aerosol over Europe. *Atmospheric Chemistry and Physics*, *13*(9), 4917–4939. https://doi.org/10.5194/acp-13-4917-2013

Renfro, A. A., Cochran, J. K., & Colle, B. A. (2013). Atmospheric fluxes of ^{7}Be and ^{210}Pb on monthly time-scales and during rainfall events at Stony Brook, New York (USA). *Journal of Environmental Radioactivity*, *116*, 114–123. https://doi.org/10.1016/j.jenvrad.2012.09.007

Ryken, N., Al-Barri, B., Blake, W., Taylor, A., Tack, F. M. G., Van Ranst, E., et al. (2018). Rapid and irreversible sorption behavior of ^{7}Be assessed to evaluate its use as a catchment sediment tracer. *Journal of Environmental Radioactivity*, *182*(November 2017), 108–116. https://doi.org/10.1016/j.jenvrad.2017.11.018

Saari, H. K., Schmidt, S., Castaing, P., Blanc, G., Sautour, B., Masson, O., & Cochran, J. K. (2010). The particulate ^{7}Be/^{210}Pb$_{xs}$ and ^{234}Th/^{210}Pb$_{xs}$ activity ratios as tracers for tidal-to-seasonal particle dynamics in the Gironde estuary (France): Implications for the budget of particle-associated contaminants. *Science of the Total Environment*, *408*(20), 4784–4794. https://doi.org/10.1016/j.scitotenv.2010.07.017

Saffari, A., Daher, N., Shafer, M. M., Schauer, J. J., & Sioutas, C. (2014). Global perspective on the oxidative potential of airborne particulate matter: A synthesis of research findings. *Environmental Science and Technology*, *48*(13), 7576–7583. https://doi.org/10.1021/es500937x

Sakata, K., Sakaguchi, A., Tanimizu, M., Takaku, Y., Yokoyama, Y., & Takahashi, Y. (2014). Identification of sources of lead in the atmosphere by chemical speciation using X-ray absorption near-edge structure (XANES) spectroscopy. *Journal of Environmental Sciences (China)*, *26*(2), 343–352. https://doi.org/10.1016/S1001-0742(13)60430-1

Sakata, K., Sakaguchi, A., Yokoyama, Y., Terada, Y., & Takahashi, Y. (2017). Lead speciation studies on coarse and fine aerosol particles by bulk and micro X-ray absorption fine structure spectroscopy. *Geochemical Journal*, *51*(3), 215–225. https://doi.org/10.2343/geochemj.2.0456

Sanchez, K., Zhang, B., Liu, H., Saliba, G., Chen, C.-L., Lewis, S., et al. (2020). Linking marine phytoplankton emissions, meteorological processes and downwind particle properties with FLEXPART. *Atmospheric Chemistry and Physics Discussions*, 1–34. https://doi.org/10.5194/acp-2020-702

Saylor, R. D., Baker, B. D., Lee, P., Tong, D., Pan, L., & Hicks, B. B. (2019). The particle dry deposition component of total deposition from air quality models: right, wrong or uncertain? *Tellus, Series B: Chemical and Physical Meteorology*, *71*(1), 1–22. https://doi.org/10.1080/16000889.2018.1550324

Seinfeld J. H. and Pandis S. N. (2016) Atmospheric Chemistry and Physics: From Air Pollution to Climate Change, Third Edition. John Wiley and Sons, Inc., Hoboken, NJ. 1119 pp.

Schuler, C.; Wieland, E.; Santschi, P. H.; Sturm, M.; Lueck, A.; Bollhalder, S.; Beer, J.; Bonani, G.; Hofmann, H. J.; Suter, M.; et al. (1991) A multi-tracer study of radionuclides in Lake Zurich, Switzerland 1. Comparison of atmospheric and sedimentary fluxes of ^{7}Be, ^{10}Be, ^{210}Pb, ^{210}Po, and ^{137}Cs. *J. Geophys. Res.*, *96* (C9), 17051–17065.

Shafer, M. M., Toner, B. M., Overdier, J. T., Schauer, J. J., Fakra, S. C., Hu, S., et al. (2012). Chemical speciation of vanadium in particulate matter emitted from diesel vehicles and urban atmospheric aerosols. *Environmental Science and Technology*, *46*(1), 189–195. https://doi.org/10.1021/es200463c

Shen, X., Saathoff, H., Huang, W., Mohr, C., Ramisetty, R., & Leisner, T. (2019). Understanding atmospheric aerosol particles with improved particle identification and quantification by single-particle mass spectrometry. *Atmospheric Measurement Techniques*, *12*(4), 2219–2240. https://doi.org/10.5194/amt-12-2219-2019

Short, D., Appleby, P., & Hilton, J. (2007). Measurement of atmospheric fluxes of radionuclides at a UK site using both direct (rain) and indirect (soils) methods. *International Journal of Environment and Pollution*, *29*(4), 392–403.

Shotyk, W., Kempter, H., Krachler, M., & Zaccone, C. (2015). Stable (^{206}Pb, ^{207}Pb, ^{208}Pb) and radioactive (^{210}Pb) lead isotopes in 1-year of growth of Sphagnum moss from four ombrotrophic bogs in southern Germany: Geochemical significance and environmental implications. *Geochimica et Cosmochimica Acta*, *163*, 101–125. https://doi.org/10.1016/j.gca.2015.04.026

Simoneit, B. R. T., & Mazurek, M. A. (1989). Organic tracers in ambient aerosols and rain. *Aerosol Science and Technology*, *10*(2), 267–291. https://doi.org/10.1080/02786828908959264

Singleton, A. A., Schmidt, A. H., Bierman, P. R., Rood, D. H., Neilson, T. B., Greene, E. S., et al. (2017). Effects of grain size, mineralogy, and acid-extractable grain coatings on the distribution of the fallout radionuclides ^{7}Be, ^{10}Be, ^{137}Cs, and ^{210}Pb in river sediment. *Geochimica et Cosmochimica Acta*, *197*, 71–86. https://doi.org/10.1016/j.gca.2016.10.007

Sportisse, B. (2007). A review of parameterizations for modelling dry deposition and scavenging of radionuclides. *Atmospheric Environment*, *41*(13), 2683–2698. https://doi.org/10.1016/j.atmosenv.2006.11.057

Staelens, J., De Schrijver, A., Van Avermaet, P., Genouw, G., & Verhoest, N. (2005). A comparison of bulk and wet-only deposition at two adjacent sites in Melle (Belgium). *Atmospheric Environment*, *39*(1), 7–15. https://doi.org/10.1016/j.atmosenv.2004.09.055

Stein, A. F., Draxler, R. R., Rolph, G. D., Stunder, B. J. B., Cohen, M. D., & Ngan, F. (2015). NOAA's hysplit atmospheric transport and dispersion modeling system. *Bulletin of the American Meteorological Society*, *96*(12), 2059–2077. https://doi.org/10.1175/BAMS-D-14-00110.1

Steinmann, P. S., Illen, T. B., Oizeau, J. L., & Ominik, J. D. (1999). Beryllium-7 as a tracer to study mechanisms and rates of metal scavenging from lake surface waters. *Environmental Science & Technology*, *63*(11), 1621–1633.

Su, C.-C. (2003). Factors controlling atmospheric fluxes of ^{7}Be and ^{210}Pb in northern Taiwan. *Geophysical Research Letters*, *30*(19), 7–10. https://doi.org/10.1029/2003gl018221

Su, C. C., & Huh, C. A. (2006). Measurements of ^{7}Be and ^{210}Pb in cloudwaters: Toward a better understanding of aerosol transport and scavenging. *Geophysical Research Letters*, *33*(4), 33–36. https://doi.org/10.1029/2005GL025042

Sugihara, S., & Momoshima, N. (2000). Variation of atmospheric ^{7}Be and ^{210}Pb depositions at Fukuoka, Japan. *IRPA 10th Congress,Hiroshima, Japan, 10-16 May 2000*.

Sumerling, T. J. (1984). The use of mosses as indicators of airborne radionuclides near a major nuclear installation. *Science of The Total Environment*, *35*, 22.

Talbot, R. W., & Andren, A. W. (1983). Relationships between Pb and ^{210}Pb in aerosol and precipitation at a semi-remote site in northern Wisconsin. *Journal of Geophysical Research*, *88*(C11), 6752–6760. https://doi.org/10.1029/JC088iC11p06752

Taylor, A., Blake, W. H., Smith, H. G., Mabit, L., & Keith-Roach, M. J. (2013). Assumptions and challenges in the use of fallout beryllium-7 as a soil and sediment tracer in river basins. *Earth-Science Reviews*, *126*, 85. https://doi.org/10.1016/j.earscirev.2013.08.002

Tipping, E, Benham, S., Boyle, J.F., Crow, P., Davies, J., et al. (2014). Atmospheric deposition of phosphorous to land and freshwater. *Environ. Sci. Procesess Impacts. 16*, 1608-1617. https://doi.org/10.1039/c3em00641g.

Todd, J. F., Wong, G. T. F., Olsen, C. R., & Larsen, I. L. (1989). Atmospheric depositional characteristics of beryllium-7 and lead-210 along the southeastern Virginia coast. *Journal of Geophysical Research*, *94*(D8), 11106–11116. https://doi.org/10.1029/JD094iD08p11106

Tokieda, T., Yamanaka, K., Harada, K., & Tsunogai, S. (1996). Seasonal variations of residence time and upper atmospheric contribution of aerosols studied with Pb-210, Bi-210, Po-210 and Be-7. *Tellus, Series B: Chemical and Physical Meteorology*, *48*(5), 690–702. https://doi.org/10.3402/tellusb.v48i5.15940

Tositti, L., Pieri, L., Brattich, E., Parmeggiani, S., and Ventura, F. (2018). Chemical characteristics of atmospheric bulk deposition in a semi-rural area of

the Po Valley (Italy). *J. Atmos. Chem. 75*, 97-121.

Toubiana, D., Fernie, A. R., Nikoloski, Z., & Fait, A. (2013). Network analysis: Tackling complex data to study plant metabolism. *Trends in Biotechnology*, *31*(1), 29–36. https://doi.org/10.1016/j.tibtech.2012.10.011

Tunved, P., Hansson, H. C., Kulmala, M., Aalto, P., Viisanen, Y., Karlsson, H., et al. (2003). One-year boundary layer aerosol size distribution data from five nordic background stations. *Atmospheric Chemistry and Physics*, *3*(6), 2183–2205. https://doi.org/10.5194/acp-3-2183-2003

Turekian, K. K., Benninger, L. K., & Dion, E. P. (1983). ^{7}Be and ^{210}Pb total deposition fluxes at New Haven, Connecticut and at Bermuda. *Journal of Geophysical Research*, *88*(C9), 5411–5415. https://doi.org/10.1029/JC088iC09p05411

Underwood, J. W., Renshaw, C. E., Magilligan, F. J., Dade, W. B., & Landis, J. D. (2015). Joint isotopic mass balance: A novel approach to quantifying channel bed to channel margins sediment transfer during storm events. *Earth Surface Processes and Landforms*, *40*(12), 1563–1573. https://doi.org/10.1002/esp.3734

Villalobos, M., Bargar, J., & Sposito, G. (2005). Mechanisms of Pb(II) sorption on a biogenic manganese oxide. *Environmental Science and Technology*, *39*(2), 569–576. https://doi.org/10.1021/es049434a

Vincent, J. C., Hill, J., Walker, M. D., Smith, S. A., Smith, S. E., & Cant, N. E. (2019). Towards a predictive capability for the resuspension of particles through extension and experimental validation of the Biasi implementation of the "Rock'n'Roll" model. *Journal of Aerosol Science*, *137*, 1–16. https://doi.org/10.1016/j.jaerosci.2019.105435

Wallbrink, P., & Murray, A. (1993). Use of fallout radionuclides as indicators of erosion processes. *Hydrological Processes*, *7*(3), 297–304. Retrieved from http://onlinelibrary.wiley.com/doi/10.1002/hyp.3360070307/abstract

Wan, G., Zheng, X., Lee, H. N., Bai, Z. Wan, E., et al. (2010) ^{210}Pb and ^{7}Be as tracers for aerosol transfers at center Guizhou, China: II. The interpretation by monthly and yearly intervals. Adv. Earth Sci., 25, 505-514. (Chinese language).

Whiting, P. J., Matisoff, G., Fornes, W., & Soster, F. M. (2005). Suspended sediment sources and transport distances in the Yellowstone River basin. *Geological Society of America Bulletin*, *117*(3), 515. https://doi.org/10.1130/B25623.1

Wieland, E., Santschi, P.H., and Beer, J. (1991) A multi-tracer study of radionuclides in Lake Zurich, Switzerland 2. Residence times, removal processes, and sediment focusing, *J. Geophys. Res. 96* (C9),17067-17080.

Willenbring, J. K., & von Blanckenburg, F. (2010). Meteoric cosmogenic beryllium-10 adsorbed to river sediment and soil: Applications for Earth-surface dynamics. *Earth-Science Reviews*, *98*(1–2), 105–122. https://doi.org/10.1016/j.earscirev.2009.10.008

Winkler, R., Dietl, F., Frank, G., & Tschiersch, J. (1998). Temporal variation of ^{7}Be and ^{210}Pb size distributions in ambient aerosol. *Atmospheric Environment*, *32*(6), 983–991. https://doi.org/10.1016/S1352-2310(97)00333-6

Wittman, H., von Blanckenburg, F., Dannhaus, N., Bouchez, J., Gaillardet, J., Guyot, J. L., et al. (2014). Journal of Geophysical Research : Earth Surface. *Journal of Geophysical Research: Earth Surface*, *120*, 2498–2528. https://doi.org/10.1002/2015JF003581

World Data Center, Sunspot Index and Long-term Solar Observations (DC-SILSO), Royal Observatory of Belgium, Brussels. http://www.sidc.be/silso/datafiles#total accessed 11/26/19

Wu, M., Liu, X., Zhang, L., Wu, C., Lu, Z., Ma, P. L., et al. (2018). Impacts of aerosol dry deposition on black carbon spatial distributions and radiative effects in the community atmosphere model CAM5. *Journal of Advances in Modeling Earth Systems*, *10*(5), 1150–1171. https://doi.org/10.1029/2017MS001219

Xu, D., Ge, B., Chen, X., Sun, Y., Cheng, N., Li, M., et al. (2019). Multi-method determination of the below-cloud wet scavenging coefficients of aerosols in Beijing, China. *Atmospheric Chemistry and Physics*, *19*(24), 15569–15581. https://doi.org/10.5194/acp-19-15569-2019

Yamamoto, M., Kofugi, H., Shiraishi, K., & Igarashi, Y. (1998). An attempt to evaluate dry deposition velocity of airborne ^{210}Pb in a forest ecosystem. *Journal of Radioanalytical and Nuclear Chemistry*, *227*(1–2), 81–88. https://doi.org/10.1007/bf02386435

Yamamoto, M., Sakaguchi, A., Sasaki, K., Hirose, K., Igarashi, Y., & Kim, C. K. (2006). Seasonal and spatial variation of atmospheric ^{210}Pb and ^{7}Be deposition: Features of the Japan Sea side of Japan. *Journal of Environmental Radioactivity*, *86*(1), 110–131. https://doi.org/10.1016/j.jenvrad.2005.08.001

Yang W., Guo, L., Chuang, C. Y., Schumann, D., Ayranov, M., & Santschi, P. H. (2013) Adsorption characteristics of 210Pb, 210Po and 7Be onto micro-particle surfaces and the effects of macromolecular organic compound. *Geochim. Cosmochim. Acta*, *107*, 47-64.

Yang, H., & Appleby, P. G. (2016). Use of lead-210 as a novel tracer for lead (Pb) sources in plants. *Scientific Reports*, *6*, 1–9. https://doi.org/10.1038/srep21707

Yi, Y., Bai, J., Liu, G., Yang, W., Yi, Q., Huang, Y., & Chen, H. (2005) Measurements of atmospheric deposition fluxes of ^{7}Be, ^{210}Pb and ^{210}Po. *Mar. Sci. 29*, 20-24. (Chinese language)

Yi, Y., Zhou, P., & Liu, G. (2007). Atmospheric deposition fluxes of ^{7}Be, ^{210}Pb and ^{210}Po at Xiamen, China. *Journal of Radioanalytical and Nuclear Chemistry*, *273*(1), 157–162. https://doi.org/10.1007/s10967-007-0728-6

Zhang, L., Yang, W., Chen, M., Zhu, Y. & Wang, Z. (2019) Atmospheric deposition of ^{210}Po and ^{210}Pb near the coast of Xiamen, Acta Oceanol. Sin., 41,

114-122. (Chinese language).

Zhang, F., Wang, J., Baskaran, M., Zhong, Q., Wang, Y., Paatero, J., & Du, J. (2021). A comprehensive global dataset of atmospheric ^{7}Be and ^{210}Pb measurements: air concentration and depositional flux. *Earth System Science Data*, *7*, 1–75. Retrieved from https://doi.org/10.5194/essd-2021-35